nature communications

Article

https://doi.org/10.1038/s41467-025-61901-z

Cardiomyocyte OTUD1 drives diabetic cardiomyopathy via directly deubiquitinating AMPKα2 and inducing mitochondrial dysfunction

Received: 20 November 2024

Accepted: 3 July 2025

Published online: 19 July 2025

Check for updates

Xue Han[1,2], Ruyi Zheng[1], Jiajia Zhang[1,3], Yanan Liu[1], Ze Li[1], Guoxuan Liu[1], Jianing Zheng[1], Weiqi Li[1], Zijun Liang[1], Mengyang Wang[4], Jie Yu[1,5], Qiaojuan Shi[1] ✉, Huazhong Ying[1] ✉ & Guang Liang[2,3,5] ✉

Deubiquitinating modification of proteins is involved in the pathogenesis of diseases. Here, we investigated the role and regulating mechanism of a deubiquitinating enzyme (DUB), ovarian tumor domain-containing protein 1 (OTUD1), in diabetic cardiomyopathy (DCM). We find a significantly increased OTUD1 expression in diabetic mouse hearts, and single-cell RNA sequencing shows OTUD1 mainly distributing in cardiomyocytes. Cardiomyocyte-specific OTUD1 knockout prevents cardiac hypertrophy and dysfunction in both type 2 and type 1 diabetic male mice. OTUD1 deficiency restores cardiac AMPK activity and mitochondrial function in diabetic hearts and cardiomyocytes. Mechanistically, OTUD1 binds to AMPKα2 subunit, deubiquitinates AMPKα2 at K60/K379 sites, and then inhibits AMPK^{T172} phosphorylation through impeding the interaction of AMPKα2 and its upstream kinase CAMKK2. Finally, silencing AMPKα2 in cardiomyocytes abolishes the cardioprotective effects of OTUD1 deficiency in diabetic mice. In conclusion, this work identifies a direct regulatory DUB of AMPK and presents a OTUD1-AMPK axis in cardiomyocytes for driving DCM.

Diabetic cardiomyopathy (DCM), a diabetes mellitus (DM)-induced pathological condition of the heart, has an independent role in boosting the incidence of heart failure (HF) regardless of hypertension, coronary artery disease, hyperlipidemia, and valvular heart disease[1,2]. In DCM, long-term hyperglycemia leads to cardiac pathological changes, including myocardial stiffness, hypertrophy, fibrosis, and the consequent cardiac systolic and diastolic dysfunction[3]. Although conventional cardiovascular drugs are available for the management of HF in diabetic patients, the clinical efficacy is still a little far from satisfaction. An in-depth understanding of the underlying mechanisms of DCM may provide effective interventions to prevent the development of this disease.

Hyperglycemia-induced energy metabolism dysfunction in cardiomyocytes is primarily manifested to contribute to the development

[1]Zhejiang Provincial Key Laboratory of Laboratory Animals and Safety Research, School of Pharmaceutical Sciences, Hangzhou Medical College, Hangzhou, Zhejiang, China. [2]Department of Cardiology, the First Affiliated Hospital, Wenzhou Medical University, Wenzhou, Zhejiang, China. [3]Zhejiang-Tailand Joint Laboratory of Cardiovascular Diseases, School of Pharmaceutical Sciences, Hangzhou Medical College, Hangzhou, Zhejiang, China. [4]Department of Pharmacology, College of Pharmacy, Beihua University, Jilin City, Jilin, China. [5]Department of Pharmacy and Institute of Inflammation, Zhejiang Provincial People's Hospital, Affiliated People's Hospital, Hangzhou Medical College, Hangzhou, Zhejiang, China. ✉e-mail: shiqiaojuan@163.com; yhz0101@126.com; wzmcliangguang@163.com

of DCM[4]. Especially, the relationship between disturbed mitochondrial homeostasis and cardiac dysfunction has been well established, since almost 95% of ATP in cardiomyocytes is derived from oxidative phosphorylation (OXPHOS) in mitochondria, sustaining cardiac excitation-contraction coupling[5,6]. Clinical studies have shown that mitochondria from diabetic hearts occur ATP deficit and poor oxygenation, which in turn increases mitochondrial reactive oxygen species (ROS) and oxidative stress[7,8]. Restoration of complex I activity relieves both mitochondrial respiratory dysfunction and DCM in streptozotocin (STZ)-induced diabetic mice[6]. AMP-activated protein kinase (AMPK), as a crucial regulator of energy homeostasis in cardiomyocytes, participates in the maintenance of mitochondrial function in DCM[9]. Studies in diabetic mice have demonstrated that the reduced AMPK activity in diabetic hearts is associated with increased mitochondrial instability and subsequently deterioration in cardiac function[10–12]. In addition, AMPK activation by small molecules significantly attenuates DCM in mouse models[13,14]. Therefore, positive regulation of AMPK activity in cardiomyocytes to maintain mitochondrial stability may be a promising therapeutic target for DCM.

Ubiquitination/deubiquitination serves as an essential mechanism for protein modification and plays a crucial role in regulating multiple biological processes[15]. The process of deubiquitination is mediated by deubiquitinating enzymes (DUBs), which reverse ubiquitination by removing ubiquitin molecules from substrate proteins[16]. DUBs are extensively implicated in various diseases, particularly in cancer and immune diseases[15,17]. DUBs also participate in the pathogenesis of cardiovascular diseases, such as hypertensive HF, obesity cardiomyopathy, and atherosclerosis[18–20]. Recently, increasing evidence has suggested that deubiquitinating modification regulation is involved in the progression of DCM[21]. USP28 has been reported to be downregulated in hyperglycemic cardiomyocytes, and restoration of USP28 alleviates DCM via deubiquitinating PPARα[21]. Considering the deep involvement of deubiquitination regulation in DCM, other DUBs in cardiac pathophysiology warrant in-depth investigation to identify attractive therapeutic targets for this disease.

Through a single-cell RNA-sequencing (scRNA-seq) analysis, this study identified that a cardiomyocyte-derived DUB, ovarian tumor (OTU) domain-containing protein 1 (OTUD1), might be a crucial factor in DCM. OTUD1 belongs to the OTU family and has been linked with cancer, immune response, and inflammation[22–24]. However, the role of OTUD1 in DCM has not been studied. This study further explored the effect of cardiomyocyte OTUD1 on DCM. Cardiomyocyte-specific OTUD1 deficiency effectively prevented DCM in both type 1 and type 2 diabetic mice. Mechanically, we identified AMPKα2 as the crucial substrate of OTUD1 by interactomes in cardiomyocytes. OTUD1 removes the K63-linked ubiquitin molecules from AMPKα2 at K60/K379 sites, which hinders the interaction between AMPK and Ca^{2+}/calmodulin-dependent protein kinase kinase2 (CAMKK2) and then inactivates AMPK to induce mitochondrial dysfunction and cardiomyocyte injuries. Our study illustrated a detrimental effect of OTUD1 and identified a cardiomyocyte-specific OTUD1-AMPK axis in mediating DCM, suggesting that targeting OTUD1 represents a potential therapy strategy for DCM.

Results

Cardiomyocyte-Derived OTUD1 is markedly upregulated in diabetic heart

To analyze the mRNA profile of DUBs in diabetic hearts, we performed a scRNA-seq of ~16,666 single heart cells from the wild-type (WT) mice and *db/db* mice (26-week-old), a typical T2DM model mouse (Fig. 1a). Among these DUBs, the *Otud1* gene showed the biggest upregulation fold (Log2FC [T2DM/Ctrl] = 1.14; Fig. 1b and Supplementary Table 1). This gene also showed the most predominant expression in cardiomyocytes among all OTU subfamily members (Supplementary Table 1). We then confirmed that both mRNA and protein levels of OTUD1 were markedly upregulated in T2DM mouse heart tissues (Fig. 1c–e), indicating its involvement in DCM pathology. To identify the cellular source of upregulated OTUD1 in diabetic heart, 7 main cell types were classified from scRNA-seq data based on the specific gene marker, including fibroblasts (FBs), cardiomyocytes (CMs), endothelial cells (ECs), smooth muscle cells (SMCs), macrophages (MPs), T cells, and B cells (Fig. 1f). Notably, the *Otud1* mRNA was predominantly distributed in CMs (Fig. 1g), and the protein level of OTUD1 was also highly enriched in primary cardiomyocytes and H9C2 cells, but not primary fibroblasts and primary macrophages (Supplementary Fig. 1a). It is worth noting that *Otud1* mRNA level was also increased in CMs isolated from *db/db* mice (Fig. 1h). Similarly, double immunofluorescence staining showed that increased OTUD1 was mainly noted in α-actinin positive cardiomyocytes, rather than vimentin positive fibroblasts (Fig. 1i). Upon high glucose (HG) and palmitic acid (PA) stimulation, OTUD1 protein expression was increased in a time-dependent manner in cultured neonatal rat primary cardiomyocytes (NRPCs; Fig. 1j), accompanied by a comparable increase in OTUD1's deubiquitinase activity (Supplementary Fig. 1b). Therefore, these data show that cardiomyocyte-derived OTUD1 is significantly upregulated in diabetic hearts and may play an important role in the development of DCM.

Cardiomyocyte-specific OTUD1 knockout ameliorates cardiac hypertrophy and dysfunction in the T2DM mice

To investigate the role of OTUD1 in DCM, we generated cardiomyocyte-specific OTUD1 knockout mice (conditional knockout, CKO) by crossing *Otud1*$^{fl/fl}$ mice and *Myh6*-cre mice (Supplementary Fig. 2a). The efficiency of OTUD1 knockout in cardiomyocytes was verified using immunoblotting (Supplementary Fig. 2b). *Otud1* CKO mice and littermate *Otud1*$^{fl/fl}$ mice were induced into T2DM using small-dose STZ (35 mg/kg) combing high-fat diet (HFD) feeding for 16 weeks (Fig. 2a). The levels of blood glucose and body weight did not differ in T2DM mice with or without *Otud1* knockout (Fig. 2b, c), while *Otud1* CKO diabetic mice showed decreased serum insulin levels compared to *Otud1*$^{fl/fl}$ T2DM mice (Supplementary Table 2). Cardiac injury markers, including serum levels of lactate dehydrogenase (LDH) and atrial natriuretic peptide (ANP), were significantly reduced in *Otud1* CKO diabetic mice, compared to those in *Otud1*$^{fl/fl}$ diabetic mice (Fig. 2d, e). Non-invasive echocardiography showed that *Otud1* CKO alleviated diabetes-induced cardiac dysfunction, as evidenced by reduction of ejection fraction (EF%) and fractional shortening (FS%), and increase of left ventricular internal diameter (LVIDd) and interventricular septal thickness (IVSD) (Fig. 2f–h and Supplementary Table 2). Consistently, *Otud1* knockout T2DM mice had small hearts and decreased heart weight to tibia length ratio compared to *Otud1*$^{fl/fl}$ T2DM mice (Fig. 2i and Supplementary Table 2). Hematoxylin and Eosin (H&E) and wheat germ agglutinin (WGA) staining revealed that the cross-section area of cardiomyocytes in *Otud1* CKO diabetic hearts was smaller than that in *Otud1*$^{fl/fl}$ diabetic hearts (Fig. 2j and Supplementary Fig. 3a). The examinations on the mRNA levels of hypertrophic genes and fibrotic genes, such as *Nppa*, *Nppb*, *Myh7*, *Acta1*, *Col1a1*, and *Tgfb1* in heart tissues showed *Otud1* CKO significantly reversed T2DM-induced heart hypertrophy and fibrosis in mice (Fig. 2k, l). Moreover, *Otud1* CKO mitigated collagen deposition in diabetic hearts, as measured by Masson's trichome staining- and Sirius red staining-positive area (Fig. 2m and Supplementary Fig. 3b). Taken together, cardiomyocyte-derived OTUD1 deficiency alleviates DCM in T2DM mice.

OTUD1 CKO alleviates DCM in the T1DM mice

We further evaluated the role of cardiomyocyte-derived OTUD1 in type 1 DCM. The T1DM mouse model was established using high-dose STZ injection (120 mg/kg; Fig. 3a). As expected, the diabetic mice exhibited elevated blood glucose and lowered body weight, while OTUD1

https://doi.org/10.1038/s41467-025-61901-z

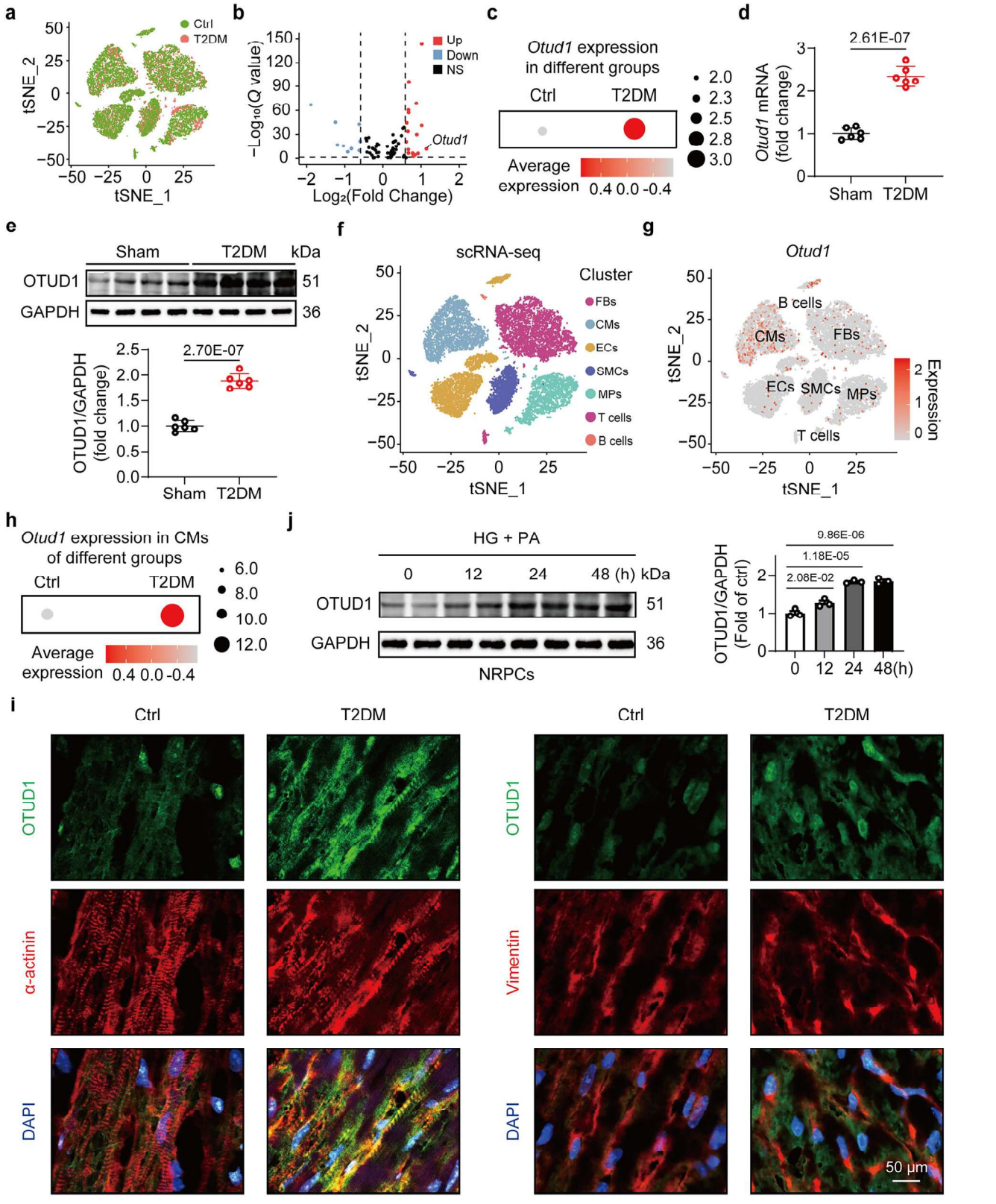

deficiency did not affect these alterations (Fig. 3b, c). Serum levels of LDH and ANP were significantly decreased in *Otud1* CKO mice with T1DM than those in *Otud1*$^{fl/fl}$ T1DM mice (Fig. 3d, e). Moreover, cardiomyocyte-specific OTUD1 deficiency led to a significant improvement of T1DM-induced cardiac dysfunction (Fig. 3f–h and Supplementary Table 3). The enlarged gross heart size and cardiomyocytes in H&E and WGA staining, and upregulated mRNA levels of hypertrophic genes were observed in T1DM mice, whereas these changes were remarkably reversed by cardiomyocyte OTUD1 deficiency (Fig. 3i–k and Supplementary Fig. 4a). Consistently, the antifibrosis effects of OTUD1 deficiency were also confirmed as evidenced by the downregulated mRNA levels of fibrotic genes and reduced interstitial fibrosis in OTUD1-deficient diabetic heart tissues (Fig. 3l, m and Supplementary Fig. 4b). These data confirm that cardiomyocyte-derived OTUD1 deficiency also attenuates T1DM-induced cardiomyopathy.

Fig. 1 | Cardiomyocyte-derived OTUD1 is markedly upregulated in hyperglycemic conditions. The single-cell RNA-sequencing (scRNA-seq) was conducted in T2DM hearts. **a** The t-SNE plot showed different cell clusters in control (Ctrl) and T2DM hearts, colored by experimental groups. **b** Volcano plot displayed the differential expression of deubiquitinating enzymes (DUBs) in heart tissues between control and T2DM mice. NS no significance. **c** Dot plot illustrated the expression levels of *Otud1* in control and T2DM hearts. **d** The mRNA levels of *Otud1* in heart tissues. **e** Representative western blot images and quantification of protein levels of OTUD1 in heart tissues. **f** The t-SNE plot identified seven main cell types, including fibroblasts (FBs), cardiomyocytes (CMs), endothelial cells (ECs), smooth muscle cells (SMCs), macrophages (MPs), T cells, and B cells in scRNA-seq analysis. **g** A biaxial scatter plot showing the expression pattern of *Otud1* across these cell clusters. **h** Dot plot indicated the relative expression of *Otud1* in the CMs. **i** Representative images of immunofluorescence staining for OTUD1 (green), DAPI (blue), α-actinin (red), or vimentin(red) in heart sections from control and T2DM mice. **j** OTUD1 protein expression in neonatal rat primary cardiomyocytes (NRPCs) treated with high glucose (HG; 33 mM) and palmitic acid (PA; 100 μM) for indicated times (0, 12, 24, and 48 h). For **i**, scale bar = 50 μm. Source data are provided as a Source Data file. Data are presented as mean ± SEM (**a**–**c**, **f**–**h**: $n = 3$; **d**, **e**: $n = 6$ for each group; **i**, **j**: $n = 3$ independent experiments); For (**d**, **e**), *P* values were determined by two-tailed unpaired *t*-test; For (**j**), *P* values were determined by one-way ANOVA followed by Tukey post hoc tests.

Loss of OTUD1 restored cardiac AMPK phosphorylation and enhanced mitochondrial OXPHOS in vivo

We next probed the intracellular signaling pathway by which OTUD1 regulates DCM using bulk RNA-sequencing analysis in the hearts of T2DM-challenged *Otud1*$^{fl/fl}$ and *Otud1* CKO mice. We found 477 downregulated and 734 upregulated differentially expressed genes in diabetic *Otud1* CKO mouse heart tissues (defined using Log2FC > 1.5 and *P* value < 0.05; Supplementary Fig. 5a). Kyoto Encyclopedia of Genes and Genomes (KEGG) and Gene Ontology (GO) analysis showed significant enrichment of signaling pathways related for diabetes, cardiac hypertrophy, AMPK, and glucose and lipid metabolism (Supplementary Fig. 5b, c). Comparative Gene Set Enrichment Analysis (GSEA) further found the upregulation of AMPK, and glucose and lipid transport in OTUD1-deficient diabetic hearts (NES > 1, *P* value < 0.05; Fig. 4a, and Supplementary Fig. 5d). Consistent with GSEA results, the expressed levels of genes regulating glucose and lipid metabolism in diabetic hearts were changed by OTUD1 knockout (Supplementary Fig. 5e). We assessed the protein expression of key metabolic regulators in mouse heart tissues. Acetyl-CoA carboxylase (ACC), a downstream target of AMPK, is a crucial regulator for fatty acid oxidation[25]. Hexokinase-1 (HK-1) plays a pivotal role in maintaining glucose homeostasis[26]. As expected, T2DM mice exhibited significant decreases in the phosphorylation levels of cardiac AMPK and ACC, and HK-1 expression, while OTUD1 deficiency in cardiomyocytes reversed these changes, indicating *Otud1* CKO improves lipid/glucose metabolism and cardiac energy (Fig. 4b). Meanwhile, GSEA and GO analysis showed that mitochondrion-related OXPHOS participated in OTUD1-mediated downstream signal pathway (Fig. 4c, and Supplementary Fig. 5f). Diabetic *Otud1*$^{fl/fl}$ mice had higher mitochondrial ROS level in heart tissues than the *Otud1* CKO mice (Fig. 4d). Electron microscopy analysis showed that mitochondrial swelling, mitochondrial ridge disappearance, and reduced score in mitochondrial morphology of heart tissues from diabetic *Otud1*$^{fl/fl}$ mice, while *Otud1* CKO mitigated T2DM-induced these changes (Fig. 4e, f). We further analyzed whether diabetes alters mitochondrial function in hearts of *Otud1*$^{fl/fl}$ and *Otud1* CKO mice. The results demonstrated that T2DM impaired the content of ATP in *Otud1*$^{fl/fl}$ mouse heart, but not in *Otud1* CKO mouse heart (Fig. 4g). Consistently, diabetes-induced the reduction levels of mitochondrial respiratory chain complex II, III, and IV in heart tissues were significantly reversed in *Otud1* CKO mice (Fig. 4h), suggesting that OTUD1 regulates the energy supply of cardiac mitochondria during diabetes. Meanwhile, the levels of mitochondrial complex I and V remained unaffected (Fig. 4h). These findings support that cardiomyocyte OTUD1 deficiency reverses AMPK dephosphorylation and mitochondrial injuries in diabetic mouse heart.

OTUD1 promotes mitochondrial injuries and hypertrophy in cardiomyocytes through negatively regulating AMPK

We then validated the OTUD1-AMPK axis in cultured cardiomyocytes under HG, combining PA stimulation (HG + PA). OTUD1 was silenced using siRNA (siOTUD1) or overexpressed by transfection of the Flag-OTUD1 plasmid (OTUD1^{OE}) in NRPCs (Supplementary Fig. 6a, b). We found that HG + PA-challenged cardiomyocytes had lower phosphorylated levels of AMPK^{T172} and ACC, and HK-1 expression, while gene silencing of OTUD1 abrogated these alterations (Fig. 5a and Supplementary Fig. 6c). Not surprisingly, OTUD1 overexpression further decreased the levels of p^{T172}-AMPK, p-ACC, and HK-1 in NRPCs challenged with HG + PA (Fig. 5a and Supplementary Fig. 6c). Flow cytometry using MitoSOX probe displayed that HG + PA evoked mitochondrial ROS production in primary cardiomyocytes, while OTUD1 knockdown inhibited ROS formation (Fig. 5b). Silencing OTUD1 also significantly inhibited HG + PA-induced reductions of ATP content and mitochondrial respiratory chain complex II, III, and IV in NRPCs (Fig. 5c, d and Supplementary Fig. 6d). No influences on the expression of complex I and V (Fig. 5d and Supplementary Fig. 6d). By contrast, OTUD1 overexpression promoted mitochondrial ROS production, and further decreased ATP content in HG + PA-challenged cardiomyocytes (Supplementary Fig. 6e, f), but not worsened the levels of complex II, III, and IV (Supplementary Fig. 6g, h). We assessed mitochondrial respiratory capacity using extracellular flux analysis and found that OTUD1 knockdown resulted in increased basal ATP production, as well as maximal respiration in NRPCs challenged with HG + PA (Fig. 5e, f). Conversely, OTUD1 overexpression worsened mitochondrial respiratory capacity after HG + PA treatment (Supplementary Fig. 6i, j).

We further examined the effects of OTUD1 on hypertrophic phenotypes of cardiomyocytes. Knockdown of OTUD1 markedly reduced the cell area of primary cardiomyocytes, while OTUD1 overexpression further increased the cardiomyocyte hypertrophy (Fig. 5g, h). Similarly, we uncovered that the mRNA levels of hypertrophic genes, including *Nppa*, *Nppb*, *Myh7*, and *Acta1*, were significantly inhibited by OTUD1 knockdown, but exacerbated by OTUD1 overexpression in HG + PA-challenged NRPCs (Fig. 5i, j). To further determine whether OTUD1 affected cardiomyocyte hypertrophy via negatively regulating AMPK activity, we constructed AMPKα2 knockout H9C2 cells using CRISPR/Cas9 technology. As expected, silencing OTUD1 did not affect the mRNA levels of hypertrophic genes in AMPKα2 knockout cells under HG + PA treatment (Fig. 5k), indicating that the pro-hypertrophic action of OTUD1 is AMPK-dependent in cardiomyocytes. These findings suggest that OTUD1 deficiency prevents cardiomyocyte hypertrophy by withstanding AMPK inactivity and mitochondrial defects in cardiomyocytes.

OTUD1 directly binds to AMPKα2

To identify the specifically targeted substrate of OTUD1 in cardiomyocytes, we performed immunoprecipitation and mass spectrometry analysis, obtaining 608 proteins potentially binding to OTUD1 (Fig. 6a). Since OTUD1 regulates diabetic cardiomyocyte hypertrophy through the AMPK pathway and mitochondrial energy metabolism, we checked the 608 potential OTUD1-binding proteins. We found that, among these 608 ones, only 4 proteins have been reported to be related with DCM, AMPK pathway, and mitochondrial energy metabolism, including AMPKα2[9,10], NRF1[27], mTOR[28], and VDAC1[29] (Fig. 6b). We then confirmed the interactions between these 4 potential substrates and OTUD1 in NRPCs, respectively. We found that only AMPKα2

https://doi.org/10.1038/s41467-025-61901-z

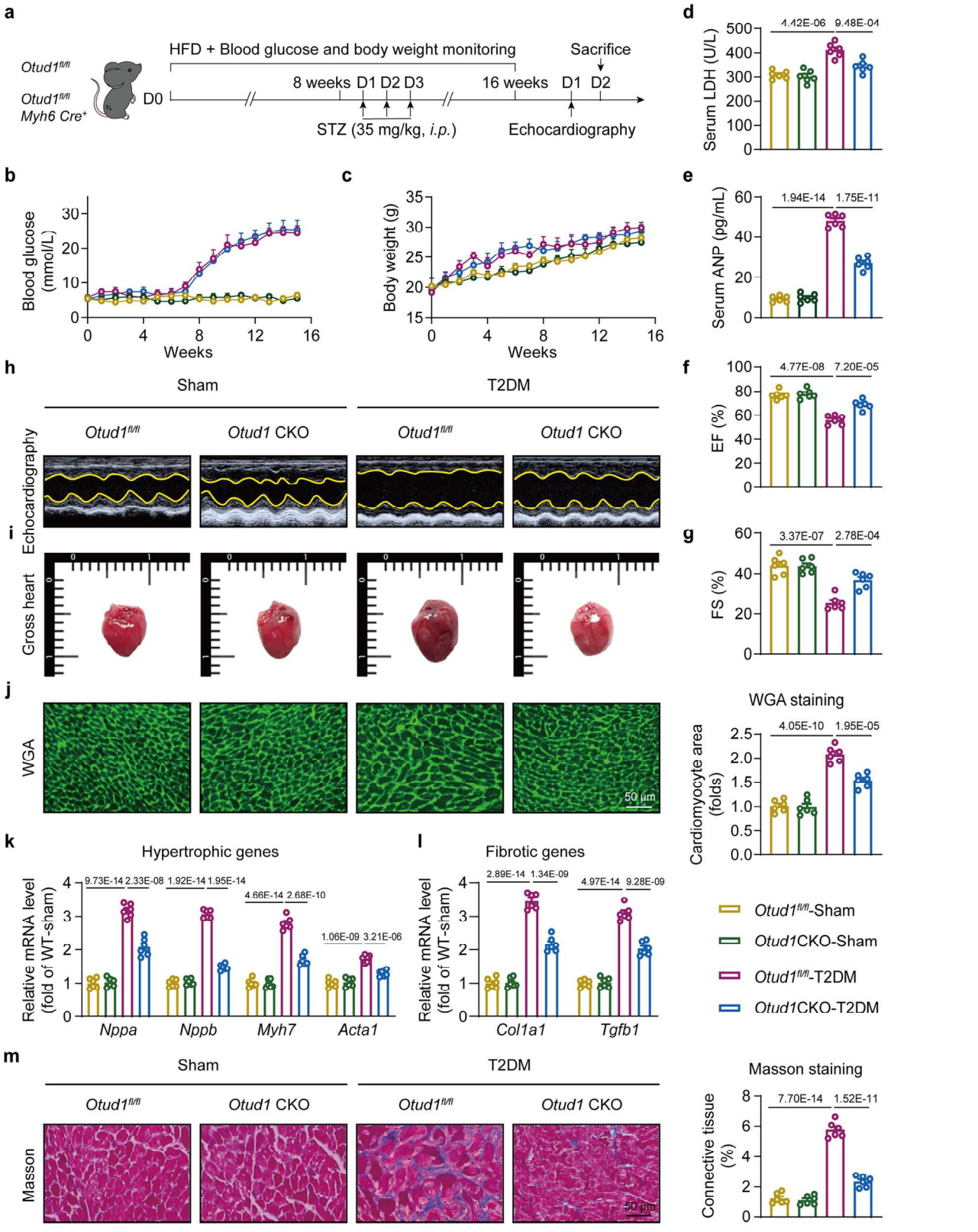

and mTOR bound to OTUD1, but NRF1 or VDAC1 showed no obvious interaction with OTUD1 in NRPCs (Supplementary Fig. 7a, b). Notably, the interaction of AMPKα2-OTUD1 but not mTOR-OTUD1 was enhanced by HG + PA stimulation in NRPCs (Supplementary Fig. 7a), suggesting that AMPKα2-OTUD1 interaction in cardiomyocytes may be more related to DCM progress. Using a co-immunoprecipitation assay, we then validated the OTUD1 interaction with AMPKα2 in diabetic heart tissues and in HG + PA-treated NRPCs (Fig. 6c, d). The immunofluorescent double-staining assay further demonstrated endogenous colocalization of OTUD1 and AMPKα2 in NRPCs after HG + PA stimulation (Fig. 6e). The exogenous interaction between OTUD1 and AMPKα2 was verified in Hek293T cells expressing Flag-OTUD1 and HA-AMPKα2 (Fig. 6f). At the cell-free molecular level, we further confirmed that rhOTUD1 protein directly bound to rhAMPK protein using bio-

Fig. 2 | Cardiomyocyte-specific OTUD1 knockout ameliorates cardiac hypertrophy and dysfunction in T2DM mice. a Schematic representation of the experimental design. *Otud1*$^{fl/fl}$ and *Otud1* cardiomyocyte-specific knockout mice were induced to T2DM by low-dose streptozotocin (STZ, 35 mg/kg) administration for 3 days combining high-fat diet (HFD) feeding for 16 weeks. After 16 weeks, the cardiac function of the mice was evaluated, and blood samples along with heart tissues were harvested. **b**, **c** Blood glucose levels and body weight of sham and T2DM mice in both *Otud1*$^{fl/fl}$ and *Otud1* conditional knockout (CKO) groups. **d**, **e** Serum levels of lactate dehydrogenase (LDH) and atrial natriuretic peptide (ANP) in different groups of mice. **f**, **g** Echocardiography was performed to assess ejection fraction (EF%) and fractional shortening (FS%). **h**, **i** Representative echocardiographic images and gross heart morphology from each group. **j** Wheat germ agglutinin (WGA) staining and quantitative analysis of cardiomyocyte area in heart tissues. **k**, **l** The mRNA levels of hypertrophic genes (*Nppa*, *Nppb*, *Myh7*, and *Acta1*) and fibrotic genes (*Col1a1* and *Tgfb1*) were quantified by RT-qPCR in heart tissues. **m** Masson's trichrome staining and quantification in heart tissues. For (**j**, **m**), scale bar = 50 μm. Source data are provided as a Source Data file. Data are presented as mean ± SEM ($n = 6$ for each group); For (**d, f**, **g**, **j**–**l**), *P* values were determined by one-way ANOVA followed by Tukey post hoc tests; For (**e**, **k**) (*Bnp*), and (**m**), *P* values were determined by Kruskal–Wallis test with Dunn post hoc tests.

layer interferometry (BLI) assay, with a high association constant (KD) of 5.56×10^{-8} M (Fig. 6g).

As we know, AMPK is an obligate heterotrimer, and composes of a catalytic subunit α (α1 or α2) and two noncatalytic subunits β (β1 or β2) and γ (γ1, γ2, or γ3) subunits. In the mammal heart, AMPKα2, β1, β2, γ1, and γ2 subunits are expressed abundantly[30]. Thus, in addition to AMPKα2, we wondered whether OTUD1 binds to other AMPK subunits. Results showed that OTUD1 only bound to AMPKα2 (Fig. 6h). To further identify the protein domains responsible for AMPKα2 and OTUD1 interaction, truncated mutants for AMPKα2 and OTUD1 were constructed, respectively. OTUD1 could interact with full-length HA-AMPKα2, domain lacking HA-autoinhibitory sequence (ΔAID; 291–376 aa), and domain lacking HA-C-terminal domain (ΔCTD; 477–521 aa), but not domain lacking HA-kinase domain (ΔKD; 16–268 aa) in Hek293T cells, indicating that OTUD1 binds to the KD fragment of AMPKα2 protein (Fig. 6i, j). As shown in Fig. 6k, OTUD1 protein contains an OTU domain and a ubiquitin-interacting motif (UIM). The immunoprecipitation assay showed that AMPKα2 interacted with the OTU domain of OTUD1 (Fig. 6l). These results confirm that the OTU domain of OTUD1 directly binds to the KD fragment of AMPKα2.

OTUD1 deubiquitinates AMPKα2 at residue K60 and K379 via its active site C320 to prevent CAMKK2-AMPK interaction and then AMPK phosphorylation

We hypothesized that OTUD1 negatively regulates AMPK activation via deubiquitinating AMPKα2. As shown in Fig. 7a, OTUD1 remarkably reduced the polyubiquitination of AMPKα2 in Hek293T cells. In vivo, OTUD1 CKO reversed AMPKα2 deubiquitination in diabetic mouse hearts (Supplementary Fig. 8a). To explore whether OTUD1 affects the stability of AMPKα2, we evaluated the protein level of total-AMPK (T-AMPK) and AMPKα2. As expected, OTUD1 overexpression did not affect the protein levels of T-AMPK and AMPKα2 in Hek293T cells or NRPCs (Fig. 7b). Consistently, we uncovered that OTUD1 markedly blocked the K63-linked ubiquitination of AMPKα2 but not K48-linked ubiquitination (Fig. 7c).

We further mapped the OTUD1-mediated deubiquitination sites of AMPKα2. Through analyzing an online ubiquitination site prediction for AMPKα2[31], we identified 4 potential sites, including K60, K379, K391, and K470, in AMPKα2 protein (Supplementary Fig. 8b, Table 4). We generated various mutants of AMPKα2 for these four sites, and found that single-site mutants of K60 and K379 slightly reduced the total ubiquitination, and the mutants including both K60 and K379 almost abolished the ubiquitination of AMPKα2 (Supplementary Fig. 8c). We further confirmed that both 2KR (including K60R and K379R) and 4KR (including all 4 site mutations) significantly abolished AMPKα2 ubiquitination levels (Fig. 7d), suggesting that these two lysine residues (K60 and K379) are responsible for AMPKα2 ubiquitination. Further, OTUD1 overexpression reduced the ubiquitination level of WT AMPKα2, but failed to affect the ubiquitination of the AMPKα2-K60R or -K379R (Fig. 7e), indicating these two lysine residues are deubiquitination sites regulated by OTUD1. We also studied the functional significance of AMPKα2 deubiquitination at K60 and K379. As shown in Fig. 7f, WT AMPK overexpression increased AMPK^{T172} phosphorylation in HG + PA-challenged cardiomyocytes, but K60R and K379R mutants failed. Consistently, K60R and K379R of AMPKα2 did not ameliorate HG + PA-induced increases in mRNA levels of hypertrophic genes in cardiomyocytes (Supplementary Fig. 8d, e). These data indicate that OTUD1 negatively regulates AMPK phosphorylation via deubiquitinating K60 and K379 on AMPKα2.

Since OTUD1 has been reported to remove ubiquitination from substrates via its catalytic motif of cysteine at the 320 site (C320)[32], we constructed a mutant OTUD1 plasmid with C320A (mutation of cysteine to alanine at C320) and evaluated the deubiquitinating ability on AMPKα2. The enzyme-dead mutant of OTUD1 could not remove the ubiquitin molecules from AMPKα2 (Fig. 7g), and the phosphorylation level of AMPK^{T172} was restored in cells transfected with OTUD1 C320A (Fig. 7h). Moreover, the C320A mutant totally abolished the OTUD1-induced upregulation of hypertrophic genes in cardiomyocytes challenged with HG + PA (Fig. 7i). These results suggest that OTUD1 regulates AMPKα2 via its C320 site.

We next tested how OTUD1-mediated deubiquitination induces the dephosphorylation of AMPKα2. CAMKK2 and liver kinase B1 (LKB1) are the upstream kinases responsible for the phosphorylation of AMPK^{T172}[33]. We examined whether OTUD1-mediated AMPKα2 deubiquitination hinders the interaction between CAMKK2 or LKB1 and AMPKα2. As shown in Fig. 7j, OTUD1 overexpression weakened the binding of AMPKα2 and CAMKK2, accompanied by the decreased level of AMPK^{T172} phosphorylation, while the binding between AMPKα2 and LKB1 was not affected. Interestingly, the OTUD1 C320A mutation induced a stronger AMPKα2-CAMKK2 interaction and a higher AMPK^{T172} phosphorylation than the WT-OTUD1 (Fig. 7k). Since Hela cells have been reported to lack LKB1 expression[34], we further confirmed that OTUD1 expression reduced AMPKα2-CAMKK2 interaction in Hela cells, without the potential interference of LKB1 (Supplementary Fig. 8f). These results indicate that OTUD1-mediated deubiquitination of AMPKα2 prevents AMPKα2-CAMKK2 interaction and then reduces AMPKα2 phosphorylation in cardiomyocytes.

Cardiac-AMPKα2 knockdown abolishes the cardioprotective effects of OTUD1 deficiency in diabetic mice

To verify whether OTUD1 deficiency improves cardiac hypertrophy through regulating AMPKα2 in mice, we constructed Adeno-Associated Virus 9 (AAV9) vector carrying *Otud1* shRNA (AAV9-sh*Otud1*) and *Ampka2* shRNA (AAV9-sh*Ampka2*) with cardiomyocyte-specific promoter *cTNT*, and administered these AAVs to *db/db* mice via tail vein injection (Fig. 8a). We confirmed that OTUD1 and AMPKα2 expressions were successfully lowered in mouse heart tissues (Fig. 8b Supplementary Fig. 9a). As anticipated, neither OTUD1 nor AMPKα2 knockdown affected the hyperglycemia and gain-body-weight profiles in *db/db* mice (Supplementary Fig. 9b, c). The serum levels of insulin, total cholesterol, triglyceride, and ANP indicate that AAV9-mediated OTUD1 knockdown in hearts significantly blunted diabetes-induced metabolic disorder and myocardial injury in *db/db* mice (Fig. 8c and Supplementary Table 5). However, knockdown of OTUD1 failed to reduce these parameters in AAV9-sh*Ampka2*-treated diabetic mice

https://doi.org/10.1038/s41467-025-61901-z

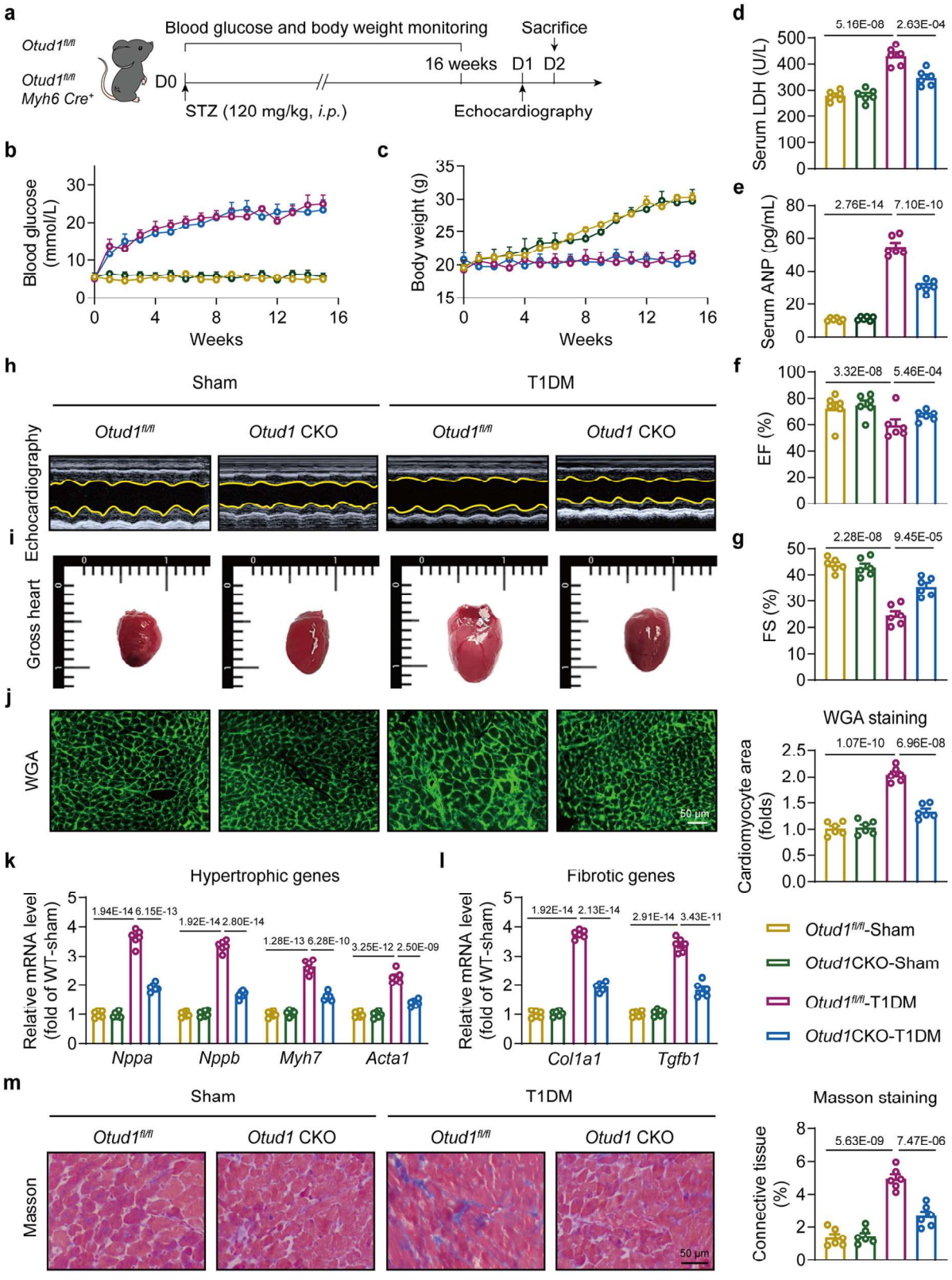

(Fig. 8c and Supplementary Table 5). OTUD1 knockdown also significantly alleviated established heart dysfunction in *db/db* mice, while AMPKα2 knockdown abolished the protective effects of OTUD1 deficiency (Fig. 8d–f and Supplementary Table 5). Analysis of hypertrophic markers and interstitial fibrosis indicators further confirmed that OTUD1 knockdown failed to prevent cardiac remodeling in AMPKα2-deficient diabetic mice (Fig. 8g–i, Supplementary Fig. 9d–g, and Table 5). Examination of the mitochondrial morphology showed that AAV9-sh*Otud1* injection attenuated mitochondrial injury in *db/db* mice, but failed in AAV9-sh*Ampka2*-treated mice (Fig. 8j, k). Subsequently, AAV9-sh*Otud1* treatment decreased mitochondrial ROS and ATP levels, and complex II, III, and IV expressions in *db/db* mice but not in AAV9-sh*Ampka2*-treated mice (Fig. 8l and Supplementary Fig. 10a–c). We also noted that OTUD1 knockdown upregulated the

Fig. 3 | Cardiomyocyte-specific OTUD1 knockout improves DCM in T1DM mice. **a** Schematic of the experimental design. *Otud1*$^{fl/fl}$ and *Otud1* conditional knockout (CKO) mice were induced to T1DM by a high dose of streptozotocin (STZ, 120 mg/kg) injection. Sixteen weeks later, cardiac function was assessed, and blood and heart tissue samples were collected. **b**, **c** Blood glucose levels and body weight were measured in sham and T1DM mice in both *Otud1*$^{fl/fl}$ and *Otud1* conditional knockout (CKO) groups for 16 weeks. **d**, **e** Serum lactate dehydrogenase (LDH) and atrial natriuretic peptide (ANP) levels in different groups of mice. **f**, **g** Statistical graphs of ejection fraction (EF%) and fractional shortening (FS%) in mice. **h**, **i** Representative images of echocardiographic and gross heart. **j** Wheat germ agglutinin (WGA) staining and quantitative analysis of heart sections. **k**, **l** The mRNA expression levels of hypertrophic genes (*Nppa*, *Nppb*, *Myh7*, *Acta1*) and fibrotic genes (*Col1a1*, *Tgfb1*) in heart tissues. **m** Masson's trichrome staining and quantification in heart tissues from different groups. For (**j**, **m**), scale bar = 50 μm. Source data are provided as a Source Data file. Data are presented as mean ± SEM ($n = 6$ for each group); For (**d**, **f**, **g**, **j**–**m**), *P* values were determined by one-way ANOVA followed by Tukey post hoc tests; For (**e**), *P* values were determined by Kruskal–Wallis test with Dunn post hoc tests.

ubiquitination level of AMPKα2 in diabetic mouse hearts (Supplementary Fig. 10d). Collectively, these results suggest that OTUD1 deficiency protects mitochondrial function and attenuates DCM via regulating AMPKα2.

Discussion

In the present study, our results delineated OTUD1 as a detrimental DUB in DCM. Cardiomyocyte OTUD1 expression was significantly increased in the hearts of T2DM mice. Cardiomyocyte-specific OTUD1 deficiency alleviated cardiac dysfunction, hypertrophy, and fibrosis in both T2DM and T1DM mice. A comprehensive RNA-seq analysis revealed that OTUD1 deficiency positively regulated AMPK signaling pathway and mitochondrial OXPHOS in diabetic mouse hearts. Mechanistically, OTUD1 K63-linked deubiquitinates AMPKα2 at K60 and K379 sites through its active site C320, which hinders the AMPK-CAMKK2 interaction and then inhibits AMPKT172 dephosphorylation. OTUD1 deficiency restored AMPK activity and then prevented mitochondrial injuries and hypertrophy in cardiomyocytes. Finally, AMPKα2 knockout blunted OTUD1 deficiency-mediated cardioprotective effects in T2DM mice. Consequently, our finding reveals an OTUD1-AMPK axis in promoting DCM pathology and provides OTUD1 as a potential therapeutic target against DCM. A schematic summary of the major findings is presented in the Graphic Abstract.

DUBs and DUB-mediated deubiquitinating modification play important roles in modulating intracellular protein stability and function, then regulating a series of pathophysiological processes[16]. Maintaining the intracellular protein quality control by ubiquitination modification is crucial in determining cardiac pathophysiology, and some E3-ubiquitin-protein ligases have been found in participating in DCM pathology[35]. However, so far, only two DUBs, USP28 and USP7 in cardiomyocytes, have been reported to play roles in DCM[21,36]. This study identified cardiomyocyte-derived OTUD1 as a vital factor involved in DCM. Interestingly, OTUD1 has attracted much attention for its roles in some cardiovascular diseases[32,37,38]. Our previous work has shown that OTUD1 deubiquitinates signal transducer and activator of transcription 3 (STAT3) to promote STAT3 phosphorylation and pathological cardiac remodeling in mice[32]. We have also revealed that OTUD1 promotes isoprenaline- and myocardial infarction-induced HF by targeting phosphodiesterase 5A[37]. Recently, Lu et al. have reported that OTUD1 regulates B cells and DC cells and participates in immune reactions in dilated cardiomyopathy[38]. Here, our scRNA-seq analysis found that among DUB genes, *Otud1* showed the highest upregulation fold in diabetic hearts. Importantly, we found that the upregulated OTUD1 was mainly distributed in cardiomyocytes, especially cardiomyocytes under diabetes or HG + PA-challenged pathological conditions. Cardiomyocyte-specific OTUD1 knockout significantly protects hearts from DCM in both T2DM and T1DM mice. Considering the specificity of OTUD1 in diabetic hearts, we believe that cardiac-specific gene therapy or small-molecule inhibitors targeting OTUD1 may be an attractive strategy for the treatment of DCM.

OTUD1 has been reported to deubiquitinate several substrate proteins, including STAT3, YAP, and RIP2, in different pathophysiological processes[24,32,39]. Here, we identified AMPK as a substrate of OTUD1. AMPK is a highly conserved heterotrimer consisting of α, β, and γ subunits[30], and our data confirm that OTUD1 binds to the kinase domain of the AMPKα2 subunit, whose expression is abundant in cardiomyocytes and has a typical activating residue Thr172[40,41]. Previous publications have always shown that diabetes or hyperglycemia inactivates cardiac AMPK at Thr172 phosphorylation[13,25]. Diabetes (sustained hyperglycemia) for more than 4 weeks starts to induce cardiac complications in mice, and the cardiac dysfunction appears after 8 weeks of sustained hyperglycemia. The changes in p-AMPK levels in diabetic heart tissues depend on the duration of diabetes. The cardiac AMPK activity is not affected during the early stage of diabetes when no cardiac complication occurs. Generally, the p-AMPK level is typically decreased in diabetic mouse hearts at a relatively long disease duration (from 8 to 28 weeks), when the hearts have been damaged by sustained hyperglycemia. Maintaining AMPK activation has been demonstrated as an effective strategy to prevent DCM[9,10,42,43]. In addition, it has been reported that high-concentration glucose represses AMPK signaling via Tripartite Motif Containing 72 (TRIM72) E3-ubiquitin-ligase-mediated AMPKα degradation and inactivation[44]. So far, no specifically designed AMPK activators have been applied in clinical trials, since the discovery of small-molecule AMPK activators is relatively difficult, and AMPK possesses opposite functions in different tissues. Metformin, a classical drug for the treatment of T2DM and known as an AMPK activator, has been reported to have a neutral effect in hearts, possibly due to its poor distribution in heart tissues and multi-target mechanisms[45,46]. Therefore, it will be interesting for treating DCM to establish a safe manner to positively regulate AMPK activity specifically in cardiomyocytes. In this study, we found that OTUD1 was mainly expressed in pathological cardiomyocytes, and OTUD1 deficiency significantly attenuated DCM through increasing AMPK^{T172} activity, indicating that targeting OTUD1 may be a strategy to activate AMPK and then treat DCM. It may be a more promising strategy for medicinal chemists to design small-molecule OTUD1 inhibitors than to design AMPK activators for the treatment of DCM.

AMPK activation is essential for metabolic homeostasis and mitochondrial bioactivity, which includes mitochondrial biogenesis, degradation, oxidative stress, and ATP generation[47]. The majority of ATP requirement in myocardium is from the mitochondrial fatty acid oxidation, and it is not surprising that the malfunctioning AMPK signaling is associated with myocardial dysfunction, hypertrophy, and even HF[9]. It has been reported that fibroblast growth factor 1 prevents DCM by elevation of mitochondrial respiration rate and fatty acid β-oxidation in an AMPK-dependent way, while these protective effects are blunted in the AMPKα2 null mice[42]. Recent studies found that the pharmacological activation of AMPK limited DCM via governing mitochondrial health[10,43]. Our results in vivo and in vitro elucidate that cardiomyocyte OTUD1 deficiency contributes to AMPK-mediated lipid/glucose homeostasis and mitochondrial OXPHOS under a hyperglycemia condition. Moreover, AMPK knockdown in cardiomyocytes abolished OTUD1-deficiency-mediated protective effects on cardiac hypertrophy and mitochondrial dysfunction. Therefore, the OTUD1-AMPK axis regulates glucose/lipid metabolism and mitochondrial bioactivity in cardiomyocytes, which represents a crucial molecular mechanism in the pathogenesis of DCM.

https://doi.org/10.1038/s41467-025-61901-z

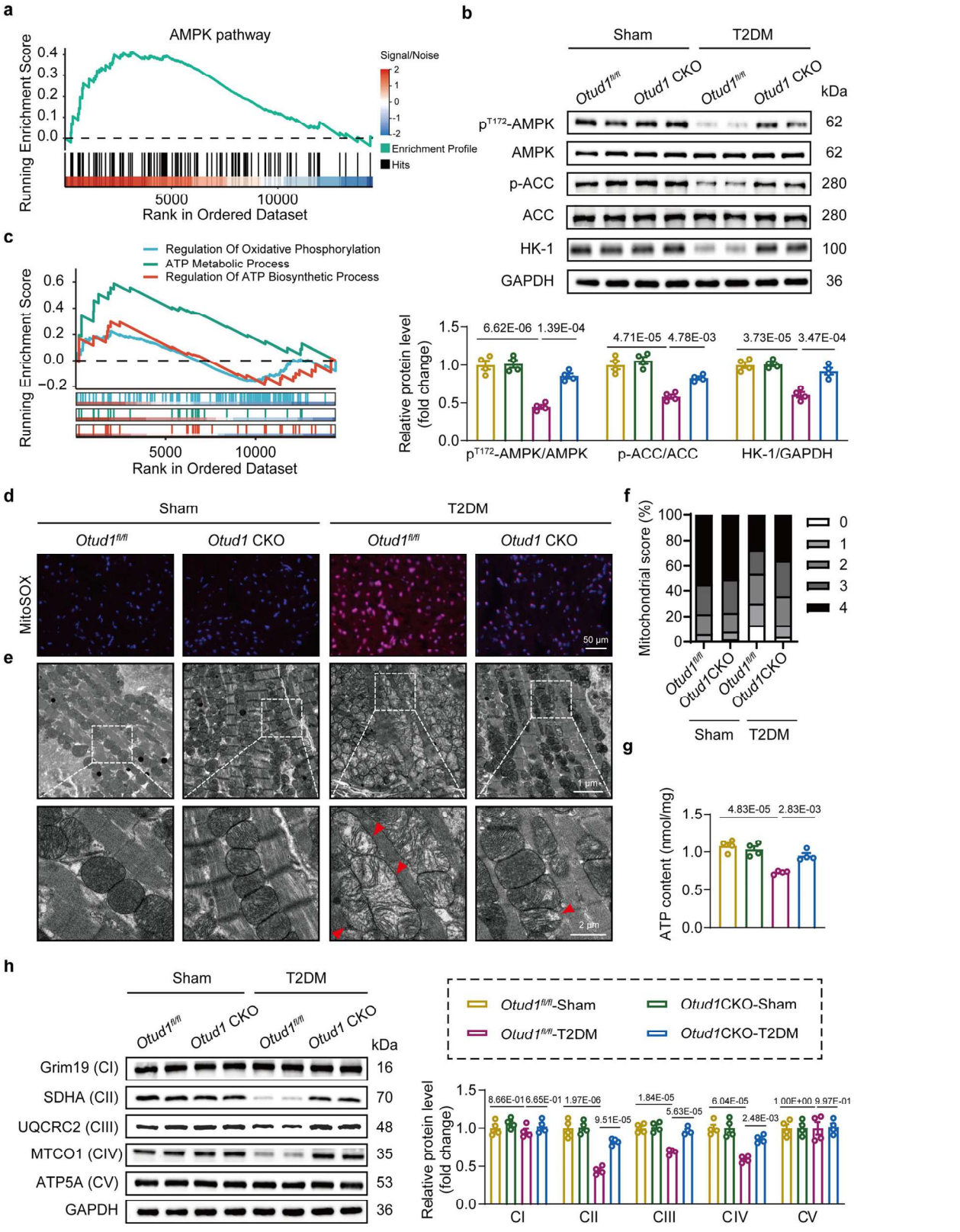

Emerging studies have implicated AMPK regulation with ubiquitin[44,48,49]. It has been shown that the ubiquitin ligase Cidea specifically interacts with the β subunit of AMPK to induce AMPK degradation in brown adipose tissues[48]. After being phosphorylated at S485/491, AMPKα recruits the E3-ubiquitin-ligase TRIM72 for the subsequent ubiquitination and degradation in high-concentration glucose-challenged skeletal muscle cells[44]. Another E3 Ligase modulator, Cereblon, has also been reported to negatively regulate AMPK signaling in skeletal muscle of type 1 diabetic rats[49]. Regarding the deubiquitinating regulation of AMPK, however, only one DUB, USP8, has been shown to be associated with AMPK activation, without a clear regulating mechanism[50]. The present study identified a direct regulating DUB of AMPK. We show that OTUD1 removes the K63-linked ubiquitin from K60 and K379 sites of AMPKα2, which prevents AMPK-CAMKK2

Fig. 4 | Loss of OTUD1 restored cardiac AMPK phosphorylation and enhanced mitochondrial OXPHOS in vivo. a, **c** Pathway enrichment analysis related to AMPK pathway and mitochondrial homeostasis by GSEA in heart tissues of T2DM-challenged *Otud1*$^{fl/fl}$ and *Otud1* conditional knockout (CKO) mice. **b** Western blot analysis and quantification of protein levels of phosphorylated AMPK (p^{T172}-AMPK), AMPK, p-ACC, ACC, and HK-1 in heart tissues from sham and T2DM mice in both *Otud1*$^{fl/fl}$ and *Otud1* CKO groups. **d** Representative images of MitoSOX staining showed mitochondrial reactive oxygen species levels in heart sections. **e** Representative images of transmission electron microscopy illustrated mitochondrial morphology in heart tissues from each group. Red arrows show abnormal mitochondria. **f** Quantitative analysis of mitochondrial morphology scores. **g** Measurement of ATP content in heart tissues from all mice. **h** Western blot analysis and quantification of mitochondrial respiratory chain complex proteins in heart tissues. For (**d**), scale bar = 50 μm; for (**e**), Scale bar = 1 μm (upper) and 2 μm (lower). Source data are provided as a Source Data file. Data are presented as mean ± SEM (**a**, **c**: $n = 4$ for *Otud1*$^{fl/fl}$ group, and $n = 3$ for *Otud1* CKO group; **b** and **d**–**h**: $n = 4$ for each group); For (**b**, **h**), *P* values were determined by one-way ANOVA followed by Tukey post hoc tests; For (**g**, **h** (CIII)), *P* values were determined by Kruskal–Wallis test with Dunn post hoc tests.

interaction and then AMPK phosphorylation at T172. It is still unclear how AMPK ubiquitinating modification regulates AMPK phosphorylation, which is crucial for AMPK activity. In this study, we find that AMPKα2 ubiquitination at K60 and K379 is necessary for AMPK-CAMKK2 interaction, providing a mechanism by which the ubiquitinating modification of AMPK regulates its phosphorylation. LKB1 is another well-established upstream kinase that phosphorylates AMPK^{T172} in myocardial cells[51]. We also show that OTUD1-mediated AMPKα2 deubiquitination does not affect AMPK-LKB1 interaction, indicating that LKB1 and CAMKK2 may interact with different domains of AMPK.

In summary, we reveal that cardiomyocyte OTUD1 deubiquitinates AMPKα2 at K60/K379 sites to inhibit AMPK^{T172} phosphorylation, promoting mitochondrial injuries and cardiomyocyte hypertrophy. This work extends our understanding of the role of DUBs in regulating AMPK activity and presents an OTUD1-AMPK axis in mediating diabetes-induced cardiomyocyte energy metabolism and DCM. Cardiomyocyte-specific OTUD1 deficiency significantly protects hearts from DCM in both T1DM and T2DM mice, suggesting that targeting OTUD1 may be an attractive therapeutic strategy for DCM.

Methods

Animal studies

All animal experiments were conducted with the approval of the Animal Care and Ethics Committee at the Zhejiang Center of Laboratory Animals, adhering to the Guide for the Care and Use of Laboratory Animals (ZJCLA-IACUC-20030091). Mice with cardiac-specific deletion of *Otud1*, generated by crossing *Otud1* floxed mice (*Otud1*$^{fl/fl}$, strain No. T005045) with α-myosin heavy chain promoter-driven heterozygous Cre (*Myh6*-Cre, strain No. T004713) mice, were purchased from Gempharmatech (Nanjing, China). *Otud1*$^{fl/fl}$ littermates served as the control group. The *db/db* mice (C57BLKS/J background) were obtained from the Laboratory Animal Center of Hangzhou Medical College (Hangzhou, China) and used as a model for T2DM. All mice used in this study were male and housed at the Laboratory Animal Center of Hangzhou Medical College. The mice were maintained in a controlled environment with a 12-h light-dark cycle, at a temperature of 22–25 °C and humidity levels of 40–70%. The animals had ad libitum access to food and water, unless otherwise specified. All animals were acclimatized for 2 weeks prior to experimentation. For all animal experiments, we selected male mice only. It has been reported that females may induce mild cardiac fibrosis and HF, because of estrogen and low testosterone levels[52].

Establishment models of diabetic cardiomyopathy

A T2DM mouse model was established by feeding male 8-week-old *Otud1*$^{fl/fl}$ Cre^{+} mice and their littermate *Otud1*$^{fl/fl}$ mice a HFD (60.3 kcal% fat, including palmitic acid, oleic acid, stearic acid, linoleic acid, and α-linolenic acid; D12492I; Research Diets, New Brunswick, USA) for 16 weeks. After 8 weeks of HFD feeding, the mice received intraperitoneal injections of STZ (35 mg/kg in citrate buffer; Sigma-Aldrich, MO, USA) for 3 consecutive days, following previously reported protocols[40]. Control mice were fed a normal diet (10 kcal% fat) and received an equivalent volume of citrate buffer via intraperitoneal injection. Six mice were included in each group.

A T1DM mouse model was established by administering a single intraperitoneal injection of STZ (120 mg/kg in citrate buffer) to male 8-week-old mice, which were then maintained on a normal diet for 16 weeks. Fasting blood glucose (FBG) levels and body weight changes were monitored weekly in both T1DM and T2DM mice. For *db/db* male mice, FBG levels were recorded starting at 8 weeks of age. For FBG assays, the mice were fasted overnight for 12 h (from 21:00 to 9:00). Blood glucose levels were measured using a glucose meter (Sano Care, Changsha, China), and mice with FBG levels above 11 mmol/L in two consecutive tests were considered diabetic mice. Six mice were included in each group. DCM was confirmed by assessing the systolic function of the heart via echocardiography. Blood and heart samples were collected for further experiments. The serum insulin level was detected by a commercial ELISA kit, and lipid levels were measured using an automatic biochemistry analyzer (Beckman).

Adeno-associated virus and viral delivery protocol

Knockdown of *Otud1* and *Ampka2* in vivo was achieved by treating *db/db* male mice with recombinant adeno-associated virus serotype 9 (rAAV9). The rAAV9 vectors contained shRNA sequences targeting the coding sequence (CDS) region of the *Otud1* gene or the *Ampka2* gene, driven by the cTnT promoter (rAAV9-cTnT-sh*Otud1* and rAAV9-cTnT-sh*Ampka2*). A rAAV9 vector carrying shRNA targeting a scrambled sequence (AAV9-Vector) was used as a control. The viral vectors were manufactured by BrainVTA (Wuhan, China). The *db/db* mice received tail vein injections of AAV9-sh*Otud1* (5×10^{11} vg, 200 μl), AAV9-sh*Ampka2* (5×10^{11} vg, 200 μl), or AAV9-Vector (200 μl). Each group included 6 mice. Knockdown efficiency of OTUD1 and AMPKα2 was assessed by western blot analysis.

Echocardiography

The day before sacrifice, transthoracic echocardiography was conducted using a VINNO 6 LAB Ultrasound Imaging System (VINNO Technology, Suzhou, China) to assess systolic and diastolic function in mice. The mice were anesthetized with 3.0% isoflurane and positioned supine on a heated platform. Isoflurane levels were adjusted to 1.0–1.5% when the mice did not respond to pressure on their hind paws, maintaining a heart rate of ~450 beats per minute. Subsequently, echocardiogram acquisition was performed. At least five consecutive cardiac cycles were recorded, and M-mode recordings were utilized for analysis of the systolic diameter of the left ventricle (LVIDs), diastolic diameter of the left ventricle (LVIDd), end-diastolic volume of the left ventricle (LVEDV), and end-systolic volume of the left ventricle (LVESV). The EF was determined using the equation EF% = (LVEDV−LVESV)/LVEDV × 100%, and the fractional shortening (FS) was calculated as (LVIDd−LVIDs)/LVIDd × 100%. Each parameter underwent measurement on a minimum of three times, and the mean value was reported.

Histological analysis

Heart tissues were harvested and fixed in 4% paraformaldehyde overnight. Subsequently, the heart tissues were dehydrated, embedded in paraffin, and transversely sliced into 5 μm-thick sections. The paraffin sections were then deparaffinized using xylene and rehydrated through a series of alcohol gradients. H&E staining was performed to

https://doi.org/10.1038/s41467-025-61901-z

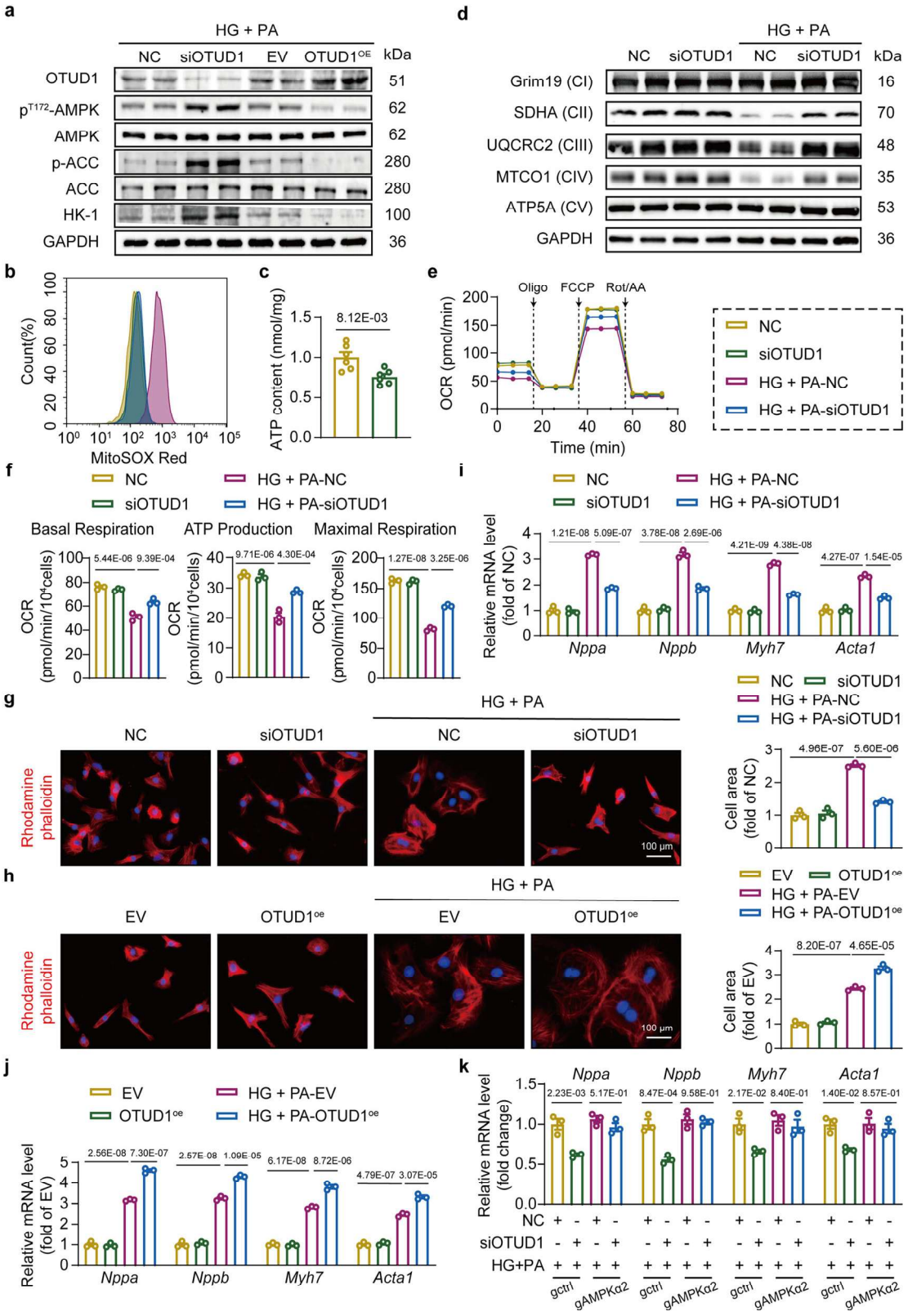

evaluate myocardial hypertrophy. The WGA staining was applied to determine the cross-sectional area size of cardiomyocytes. For the assessment of fibrosis using Masson's trichrome staining, the sections were stained with a Masson Trichrome kit (G1006, Servicebio, Wuhan, China) according to the manufacturer's instructions. Collagen deposition was evaluated on the Sirius red-stained sections. After staining, cardiac sections were analyzed under a light microscope (Leica, Wetzlar, Germany) and images were acquired. ImageJ software (NIH, Bethesda, MD, USA) was employed for quantifying the level of cardiomyocyte area, fibrosis, and collagen deposition.

Immunofluorescence analysis

Immunofluorescence staining was conducted on mouse heart samples. The heart samples were positioned flat in a specialized container,

Fig. 5 | OTUD1 promotes mitochondrial injury and hypertrophy in cardiomyocytes through negatively regulating AMPK. a Neonatal rat primary cardiomyocytes (NRPCs) transfected with siRNA targeting OTUD1 (siOTUD1), scrambled negative control (NC), OTUD1 plasmids ($OTUD1^{OE}$), or empty vector (EV) for 24 h, and were subsequently stimulated with high glucose (HG; 33 mM) and palmitic acid (PA; 100 μM) for 2 or 24 h. The expressions of OTUD1, p^{T172}-AMPK, AMPK, p-ACC, ACC, and HK-1 were detected. **b** NRPCs transfected with siOTUD1 or NC were stimulated with HG, combining PA for 1 h. Flow cytometry analysis of the mitochondrial reactive oxygen species levels in NRPCs. **c** After 24 h of HG + PA stimulation, the ATP content was detected in NRPCs. **d** Western blot analysis of mitochondrial respiratory chain complexes (Grim19, SDHA, UQCRC2, MTCO1, and ATP5A) in NRPCs. **e**, **f** Analysis of oxygen consumption rate (OCR) in NRPCs treated as indicated. Oligo oligomycin, FCCP carbonyl cyanide 4-(trifluoromethoxy) phenylhydrazone, Rot/AA rotenone/antimycin A. **g**, **i** Representative images of rhodamine phalloidin staining for cardiomyocyte area measurement. **h**, **j** RT-qPCR analysis of hypertrophic genes (*Nppa*, *Nppb*, *Myh7*, *Acta1*) in NRPCs with HG + PA stimulation for 24 h. **k** RT-qPCR analysis of hypertrophic genes in AMPKα2 knockout H9C2 cells (*gAMPKα2*) or control (*gctrl*) cells challenged with HG and PA for 24 h. For (**g**, **i**), scale bar = 100 μm. Source data are provided as a Source Data file. Data are presented as mean ± SEM (**a**, **b**, **d**–**k**: $n = 3$ independent experiments; **c**: $n = 6$ independent experiments); For (**c**), *P* values were determined by two-tailed unpaired *t*-test; For (**f**–**k**), *P* values were determined by one-way ANOVA followed by Tukey post hoc tests; For (**f**) (ATP Production), *P* values were determined by Kruskal–Wallis test with Dunn post hoc tests.

and an appropriate amount of OCT embedding medium (4583, Sakura, California, USA) was added to ensure complete submersion. The tissues were then rapidly frozen using dry ice. Once the tissues were fully frozen, they were transferred at a cold-temperature microtome (CryoStar NX70, Epredia, Shanghai, China) for sectioning, with slice thickness set at 6 μm. The sections were mounted onto glass slides and immediately fixed in 4% paraformaldehyde for 15 min. After fixation, the sections were rinsed three times with phosphate buffer solution (PBS), each rinse lasting 5 min. Excess liquid was carefully removed by gentle shaking, and the tissue boundaries were marked with an IHC pen. The sections were then treated with 5% goat serum and incubated at room temperature for 30 min. Co-staining of OTUD1 and α-actinin was achieved using a four-color fluorescence kit (RC0086, Recordbio Biological Technology, Shanghai, China) via tyramide signal amplification technology, following the provided instructions. Primary antibodies were incubated with the sections overnight at 4 °C: OTUD1 (1:100 dilution; bs-17563R, Bioss, Beijing, China), α-actinin (1:100 dilution; ab137346, Abcam, Cambridge, UK), and Vimentin (1:100 dilution; ab8978, Abcam). This process was followed by incubation with Cy3-conjugated goat anti-rabbit IgG (1:300 dilution; GB21303, Servicebio) and Alexa Fluor® 488-conjugated goat anti-rabbit IgG (1:300 dilution; GB25303, Servicebio) for 1 h at room temperature. Subsequently, the slides were cleaned with PBS, stained with DAPI for 10 min, and mounted using an anti-fluorescence quenching blocking reagent. Imaging was conducted using a confocal microscope (magnification: 200×; A1R-SIM-STORM, Nikon, Tokyo, Japan).

Total superoxide levels in tissues were assessed using the MitoSOX Red indicator (S0061, Beyotime, Shanghai, China). Briefly, frozen sections with a thickness of 10 μm were prepared and allowed to equilibrate at room temperature. A pre-cooled cleaning solution (Reagent A) was added to ensure complete coverage of the section surface before it was discarded. Subsequently, a preheated staining solution was applied at room temperature, ensuring it covered the entire section. The sections were then incubated in a humidified incubator at 37 °C for 10 min in the dark, after which the staining solution was discarded. The sections were washed with Reagent A. Finally, coverslips were sealed, and the sections were immediately observed under a confocal microscope. Enhanced red fluorescence indicates a high content of superoxide anion.

Transmission electron microscopy (TEM) analysis

The morphology and structure of mitochondria in mouse hearts were examined using TEM (HT7800, Hitachi, Tokyo, Japan). Briefly, heart pieces measuring 1.0 mm^3 from the left ventricular wall were fixed in a solution of 1.25% glutaraldehyde and 0.1 M sodium cacodylate buffer overnight at 4 °C. Subsequently, the samples underwent a series of washes in 0.1 M sodium cacodylate. After dehydration and embedding, the samples were sliced into sections with a thickness of 90 nm. These thin sections were stained with uranyl acetate and lead citrate before being observed. Digital images of the mitochondria were subsequently captured. Higher magnification images obtained from TEM revealed damaged mitochondria in diabetic hearts.

Real-time quantitative PCR (RT-qPCR)

Tissues and cellular RNA were isolated with RNAiso Plus (Takara, Tokyo, Japan). One μg of RNA was reverse transcribed into complementary DNA (cDNA) using Hifair® III 1st Strand cDNA Synthesis SuperMix (YEASEN, Shanghai, China). Subsequently, RT-qPCR was conducted on the CFX96 System (Bio-Rad, California, USA) using SYBR Green Master Mix (YEASEN). The primers utilized in this study are detailed in Supplementary Table 6. Data on the target mRNA were evaluated using the $2^{-\Delta\Delta Ct}$ method and were normalized against the expression of *β-actin*.

Bulk RNA-sequencing analysis

Total RNA from cardiac tissues ($n = 4$ for $Otud1^{fl/fl}$ group, and $n = 3$ for *Otud1* CKO group) was isolated using RNAiso Plus. Quality assessment of the RNA samples was carried out using the Agilent Bioanalyzer 2100 (Agilent Technologies, Santa Clara, USA). Purification of mRNA from 1 μg total RNA was conducted with magnetic beads attached to Oligo(dT). The purified mRNA was fragmented using a specific temperature buffer. These fragments of RNA were converted into cDNA through reverse transcription primed with random hexamers. Subsequent steps included the construction of a cDNA library and sequencing on the BGISEQ-500 platform (Beijing Genomics Institute, Shenzhen, China). Alignment of high-quality reads to the mouse reference genome was performed using Bowtie2 (v2.2.5) and Hisat2 (v2.0.4). Expression levels of genes were normalized to fragments per kilobase of exon model per million mapped reads (FPKM) utilizing RSEM (v1.2.12). Differential expression analysis was carried out using DESEQ2 (version 1.4.5) to identify genes with |fold change| > 1.5 and false discovery rate (FDR) < 0.05. Pathway analysis of KEGG and GO terms was conducted through the R package "Clusterprofile."

scRNA-seq analysis

Single-cell suspension preparation. The tissue samples were washed with PBS, minced into small fragments, and digested with enzyme solution at 37 °C with continuous shaking for about 40 min. To maximize cell yield and viability, dissociated cells were harvested at 20 min intervals during the digestion process. After digestion, Dulbecco's modified Eagle's medium (DMEM; Gibco, Eggenstein, Germany) containing 10% fetal bovine serum (FBS; Gibco) was added to the samples to stop the digestion. The cell suspension was then filtered through a 70 μm cell strainer to remove undigested tissue mass and washed with PBS containing 0.04% bovine serum albumin (Sigma). For each experimental group, three samples were pooled to generate a single biological replicate for subsequent experiments.

Reads processing. Raw data were processed using the Cell Ranger 7.2.0 sequence workflow with default and suggested settings. FASTQ files from Illumina sequencing were aligned to the mouse genome, version GRCm38, using the STAR algorithm. Gene-Barcode arrays were then generated for each sample by counting Unique Molecular Identifiers (UMIs) and excluding non-cellular-associated barcodes.

https://doi.org/10.1038/s41467-025-61901-z

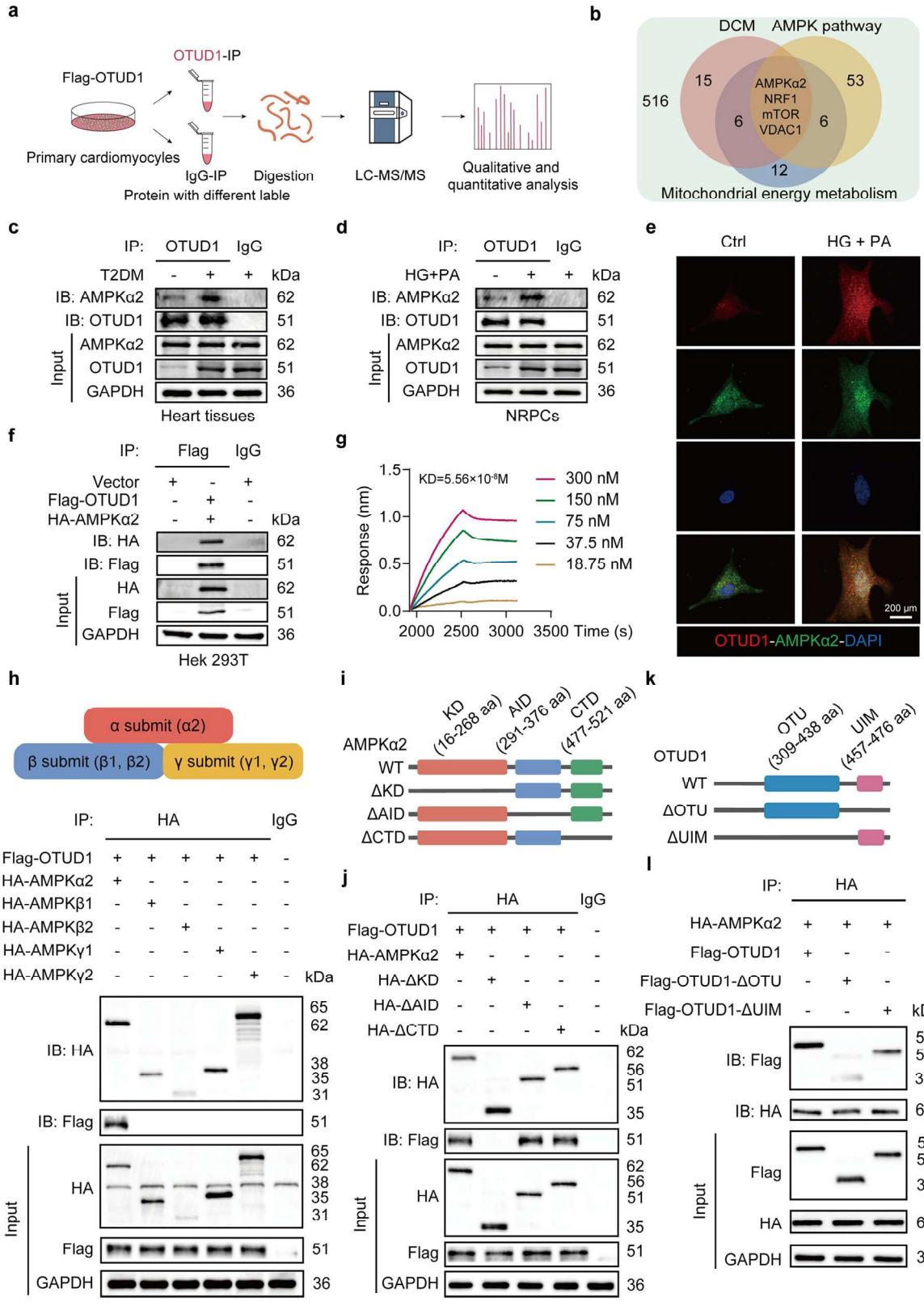

This process resulted in gene-barcode arrays encapsulating the encoded cells and gene expression counts. This output was subsequently imported into the Seurat (v4.1.1) R package for quality control and further analysis of our scRNA-seq data.

Cell filtering. All procedures were executed using default parameters, unless specified otherwise. We refined the filter to cells based on three quality criteria, including UMI count, count of detected genes, and mitochondria read percent within the Seurat package. The factors were closely associated, and finally, we requested a minimum of 500 detected genes in a cell, at least 10 cells for a gene to be detected as thresholds, and the mitochondria read percent not to exceed 25%. In total, 2727 cells were filtered away in this step, and 16,666 cells were kept for downstream analysis.

Fig. 6 | OTUD1 directly interacts with AMPKα2. a Schematic illustration of a quantitative proteomic screen to identify proteins binding to OTUD1. **b** Venn diagram represents potential OTUD1-binding proteins associating with DCM, AMPK pathway, and mitochondrial energy metabolism. **c**, **d** Co-immunoprecipitation (Co-IP) of the interaction between OTUD1 and AMPKα2 in heart tissues of T2DM mice and in high glucose (HG; 33 mM) + palmitic acid (PA; 100 μM)-treated neonatal rat primary cardiomyocytes (NRPCs). **e** Immunofluorescence staining revealed the colocalization of OTUD1 and AMPKα2 in NRPCs treated with HG + PA for 12 h. **f** Co-IP analysis confirmed the interaction between OTUD1 and AMPKα2 in Hek293T cells co-transfected with plasmids expressing Flag-OTUD1 and HA-AMPKα2. **g** Bio-layer interferometry (BLI) assay demonstrated the interaction between OTUD1 and AMPK protein, with AMPK added at different concentrations ranging from 18.75 to 300 nM, and KD values were calculated. **h** Co-IP of OTUD1 and different subunits of AMPK in Hek293T cells. **i** Schematic diagram of truncated mutants of AMPKα2. KD kinase domain, AID autoinhibitory sequence domain, CTD carboxyl-terminal domain. **j** Co-IP of OTUD1 and either wild-type AMPKα2 (HA-AMPKα2) or mutants-AMPKα2 in Hek-293T cells. **k** Schematic diagram of truncated mutants of OTUD1. OTU motif named as ovarian tumor, UIM ubiquitin-interacting motif. **l** Co-IP of AMPKα2 and either wild-type OTUD1 or mutants-OTUD1. For (**e**), scale bar = 200 μm. Source data are provided as a Source Data file. Data are presented as mean ± SEM ($n = 3$ independent experiments).

Single-cell clustering. The data were normalized using the Normalize Data function in Seurat, and a subset of variable genes was isolated. Following this, data from different samples were integrated by identifying "anchors" between datasets using the Find Integration Anchors and Integrate Data functions in Seurat. Principal Component Analysis (PCA) was performed, and the data were reduced to the top 20 PCA components following data scaling. The top 20 PCA components were used to do SNN clustering with a resolution value of 0.8. The clustering was conducted via the Seurat package (v4.1.1). Then, the canonical correlation analysis (Harmony) method in Seurat was applied to minimize batch effects among samples and experiments. Finally, clusters were visualized in a 2D representation created with t-distributed stochastic neighbor embedding (t-SNE).

NRPCs isolation and cell culture

Primary cardiomyocytes were isolated from neonatal Sprague-Dawley rats (1–2 days old). In brief, the hearts were aseptically removed from the rats, and any remaining blood was flushed out with PBS. Ventricular tissues were carefully separated from the atrium and then cut into 1 mm^3 fragments. A solution for tissue digestion was done by mixing the following components in 200 mL of double-distilled water: 0.16 g of Trypsin (T8150, Solarbio, Beijing, China), 0.07 g of sodium bicarbonate (A100865, Sangon Biotech, Shanghai, China), 1.6 g of sodium chloride (A610476, Sangon Biotech), 0.198 g of glucose (A501991, Sangon Biotech), 0.4 g of HEPES (A600264, Sangon Biotech), and 0.059 g of potassium chloride (A100395, Sangon Biotech). The solution was filtered after being dissolved. The cardiac tissues underwent digestion with the solution at 37 °C for 8 min. Following 8-10 cycles of digestion, all supernatants, excluding the initial one, were collected. These supernatants were then combined with DMEM (Gibco) that contained 20% FBS (Gibco) and a penicillin-streptomycin solution to halt the process. The cells were centrifuged at 600 g for 10 min, resuspended in DMEM with 10% FBS, passed through a 70 μm cell filter, and subsequently placed in a 37 °C incubator with 5% CO_2. After 1.5 h of incubation, the adherent cells were identified as cardiac fibroblasts. The culture medium was removed and centrifuged at 600 g for 10 min. The cell sediment was collected and resuspended in DMEM medium containing 10% FBS. After an additional 24 h, the adherent cells were cardiomyocytes, which were subsequently utilized for further experimentation. Cells were starved for 8 h and then randomly divided into two groups: 33 mM D-glucose (G8270, Sigma-Aldrich) plus 100 μM palmitic acid (PA) as the HG + PA group, and 5.5 mM D-glucose as the control group.

Hek293T cells and Hela cells were sourced from the Shanghai Institute of Biochemistry and Cell Biology (Shanghai, China). These cells were grown in DMEM with 10% FBS. Cells were cultured in an incubator at 37 °C and 5% CO_2.

Transfection of plasmids and small interfering RNA (siRNA)

Cells were transfected with plasmids to induce OTUD1 or AMPKα2 overexpression, using pcDNA3.1 vector as a control (Unibio, Chongqing, China). Plasmid transfection was carried out using the jetPRIME kit (114-15, Polyplus, Strasbourg, France) according to the manufacturer's instructions. siRNA targeting OTUD1 (5′-GGUGCAAGCAAACCCAAAUTT-3′; and 5′-AUUUGGGUUUGCUUGCACCTT-3′), AMPKα2 (5′-GAGAGCAUGAAUGGUUUAATT-3′ and 5′-UUAAACCAUUCAUGCUCUCTT-3′), or AMPKα1 (5′-GACCCGUCUUAUAGUUCAATT-3′; and 5′- UUGAACUAUAAGACGGGUCTT-3′) was transfected into cells using the jetPRIME kit (GenePharma, Shanghai, China), with scramble siRNA serving as a negative control. A total of 5 μg of plasmid DNA or 60 nM siRNA was diluted in 500 μL of jetPRIME buffer, followed by the addition of 10 μL of jetPRIME reagent. The mixture was vortexed, centrifuged, and incubated for 10 min at room temperature. The transfection mixture was then applied to cells in fresh medium for 6 h, followed by a change to complete growth medium for 24 h at 37 °C in a 5% CO2 incubator.

TRITC-phalloidin staining

Cells were seeded in 24-well plates containing round glass slides that were pre-cleaned with PBS at 37 °C, followed by fixation in 10% paraformaldehyde at room temperature for 15 min. After washing away excess formaldehyde with PBS, cells were permeabilized with 0.1% Triton X-100 for 20 min. Cells were then incubated with TRITC-labeled Phalloidin (CA1610, Beijing Solarbio Science & Technology Co., Ltd, Beijing, China) in the dark for 30 min at room temperature. Nuclei were subsequently stained with DAPI and sealed with an anti-fluorescence quenching agent. The samples were observed and imaged under a fluorescence microscope.

Assay for deubiquitinase activity of OTUD1

The deubiquitinating activity of OTUD1 was performed using an assay kit (BKDU014-096, Biortus, Wuxi, China), which used a fluorescent universal ubiquitin substrate (Ubiquitin-Rhodamine 110). The assay was conducted according to the manufacturer's instructions with minor modifications. Briefly, NRPCs were lysed in ice-cold DUB assay buffer containing 1 mM DTT at 4 °C using a Dounce homogenizer. Following centrifugation at 12,000 × g for 15 min, the supernatant was collected and immunoprecipitated with anti-OTUD1 antibody overnight at 4 °C. Subsequently, the protein A/G agarose beads (P2055, Beyotime) were added to the complexes and mildly agitated at 4 °C for 4 h. After adding the substrate mix, the relative fluorescence units were measured using a microplate reader (Bio-Rad, USA) at 485 nm excitation and 535 nm emission for a duration of at least 20 min to analyze the deubiquitinating activity of OTUD1.

ATP detection

ATP production was quantified using an ATP assay kit (S0026, Beyotime). Heart tissue (20 mg) was homogenized in 200 μL of lysis buffer using a glass homogenizer. The resulting lysates were combined with 200 μL of lysis solution to ensure complete cell disruption. Lysates were centrifuged at 12,000 × g for 5 min at 4 °C. The supernatant was then added to 100 μL of ATP detection reagent in 96-well plates, and ATP levels were measured using a luminometer.

https://doi.org/10.1038/s41467-025-61901-z

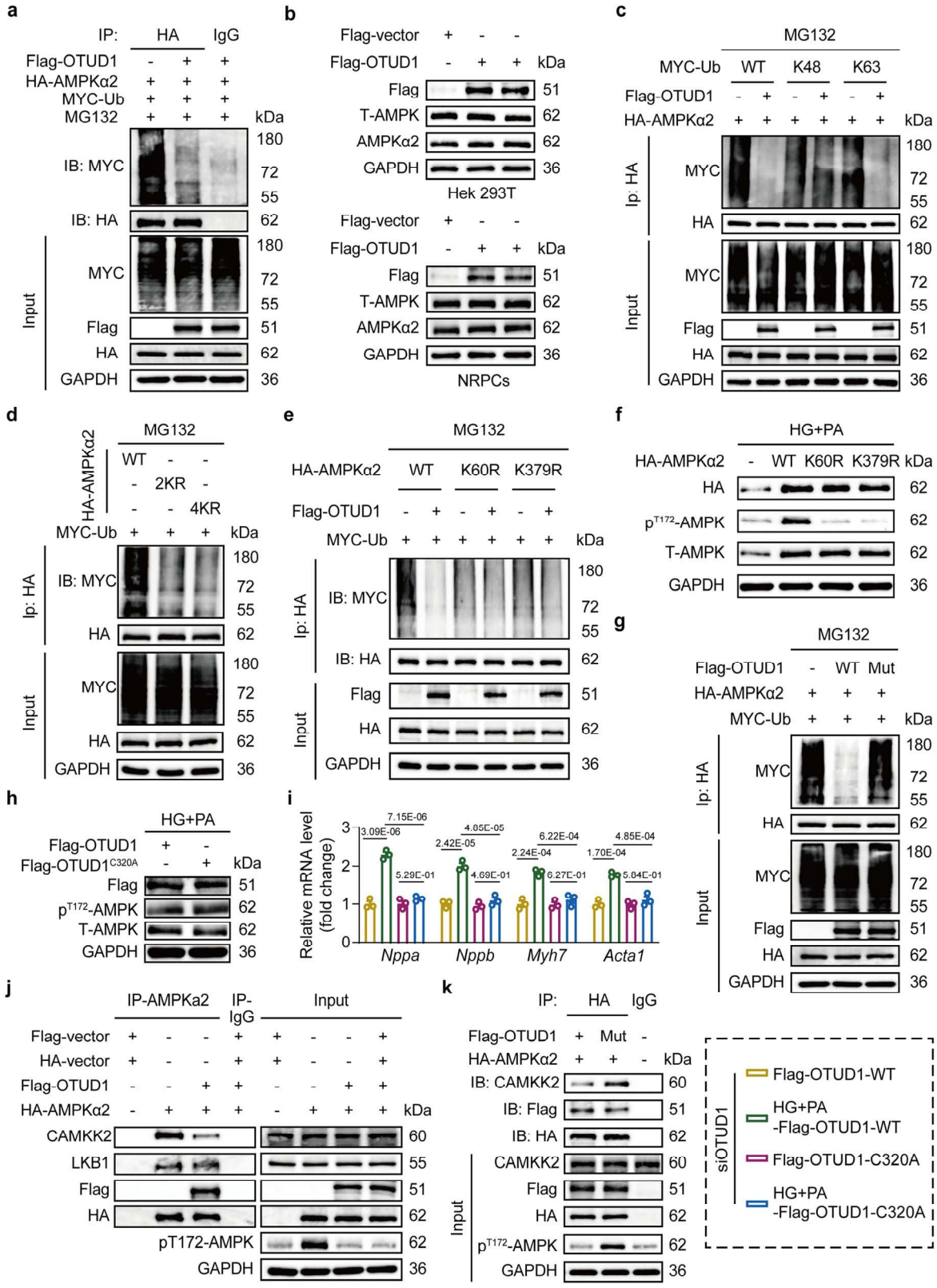

Flow cytometry assay

Mitochondrial superoxide levels in cells were assessed using the MitoSOX reagent (Beyotime). Briefly, the mitochondrial ROS in NRPCs was evaluated by flow cytometry. Primary cardiomyocytes were seeded on 6-well plates. After pre-treatment, cells were collected in a 15-mL centrifugal tube and incubated with MitoSOX reagent for 30 min at 37 °C. Then, the cells were washed with cold PBS and analyzed immediately using a FACSCelesta flow cytometer (BD, Franklin Lakes, NJ, USA). Data were analyzed using FlowJo V10 software (FlowJo, Ashland, OR, USA).

Cellular immunofluorescence assay

Immunofluorescence staining was performed to validate the colocalization of OTUD1 and AMPKα2 in NRPCs. Briefly, cells on coverslips

Fig. 7 | OTUD1 regulates the phosphorylation of AMPK by its deubiquitination activation. a Hek-293T cells were co-transfected with HA-AMPKα2, Flag-OTUD1, and MYC-ubiquitin (MYC-Ub), followed by treatment with 10 μM MG132 for 6 h. Ubiquitinated AMPKα2 was detected via immunoblotting. **b** Western blot analysis of total AMPK (T-AMPK) and AMPKα2 in Hek-293T cells (upper), transfected with Flag-OTUD1 plasmids, as well as in NRPCs (lower). **c** Co-immunoprecipitation (Co-IP) assay demonstrated the ubiquitination of AMPKα2 by K48-Ub or K63-Ub in Hek-293T cells. **d** Co-IP assay was conducted in Hek-293T cells co-transfected with HA-AMPKα2 (WT) or mutants carrying lysine-to-arginine substitutions at two sites (K60R and K379R) or four sites (K60R, K379R, K391R, and K470R), and MYC-Ub plasmids to determine AMPKα2 ubiquitination levels. **e** Ubiquitination levels of AMPKα2 were assessed in Hek-293T cells co-transfected with WT HA-AMPKα2, HA-AMPKα2-K60R, or HA-AMPKα2-K379R, and MYC-Ub plasmids. **f** Western blot analysis was performed to evaluate phosphorylated AMPK (p^{T172}-AMPK) and total AMPK in NRPCs transfected with WT, K60R, or K379R AMPKα2 under high glucose (HG; 33 mM) and palmitic acid (PA; 100 μM) stimulation for 2 h. **g** Co-IP assay was used to analyze ubiquitinated AMPKα2 in Hek-293T cells co-transfected with WT-OTUD1 or the 320 cysteine mutant to alanine (C320A; OTUD1-Mut), and MYC-Ub plasmids. **h** Western blot analysis of p^{T172}-AMPK and T-AMPK in NRPCs over-expressing WT-OTUD1 or C320A-OTUD1 under HG and PA stimulation for 2 h. **i** RT-qPCR analysis of hypertrophic genes in NRPCs challenged with HG + PA for 24 h. **j** Co-IP of CAMKK2, LKB1, and p^{T172}-AMPK in Hek-293T cells treated as indicated. **k** CAMKK2 and p^{T172}-AMPK levels were analyzed in Hek-293T cells overexpressing WT-OTUD1, Mut-OTUD1, and MYC-Ub. Source data are provided as a Source Data file. Data are presented as mean ± SEM ($n = 3$ independent experiments); For (**i**), *P* values were determined by one-way ANOVA followed by Tukey post hoc tests.

were fixed with 10% paraformaldehyde for 15 min at room temperature. After fixation, the cells were permeabilized with 0.1% Triton X-100 for 20 min, followed by blocking with 5% goat serum for 1 h. The co-staining of OTUD1 and AMPKα2 was carried out using a four-color fluorescence kit. The cells were incubated overnight at 4 °C with primary antibodies for OTUD1 (1:100 dilution) and AMPKα2 (1:100 dilution; MA5-37501, Invitrogen, CA, America), and subsequently treated with secondary antibodies including Cy3-conjugated goat anti-rabbit IgG (1:300 dilution) and Alexa Fluor® 488-conjugated goat anti-rabbit IgG (1:300 dilution) for 1 h at 37 °C. DAPI was used to stain the nuclei for 20 min, and fluorescence images were captured using a confocal microscope.

Liquid chromatography tandem mass spectrometry (LC-MS/MS) analysis

The Flag-OTUD1 plasmid was transfected into NRPCs. NRPCs lysates were subjected to IP with the Flag antibody (20543-1-AP, Proteintech). Rabbit IgG served as the negative control (each group contained one sample). Subsequently, LC-MS/MS analysis was performed by PTM Bio Co., Ltd. (Hangzhou, China). Briefly, precipitated proteins were in-gel digested by adding 1% trypsin and incubating at 37 °C overnight into peptides. The mobile phase was prepared with Buffer A (0.1% formic acid and 2% acetonitrile in MS water) and Buffer B (0.1% formic acid and 2% water in MS acetonitrile). Peptides were separated with a linear gradient from 3% to 80% Buffer B over 46 min, and all at a constant flow rate of 500 nl/min on a NanoElute UHPLC system (Bruker Daltonics, Billerica, USA). The peptides were ionized via a capillary source and analyzed using a timsTOF Pro mass spectrometer (Bruker Daltonics) in data-independent parallel accumulation serial fragmentation (DIA-PASEF) mode. The electrospray voltage was set to 1.75 kV. The full MS scans ranged from 300 to 1500, and MS/MS scans (400–850) were acquired at a rate of 20 PASEF scans per cycle with a 7 *m/z* isolation window. Precursors and fragments were detected using a TOF detector. The DIA data were processed using the DIA-NN search engine (v.1.8). Tandem mass spectra were searched against the "Homo_sapiens_9606_SP_20231220.fasta (20,429 entries)" concatenated with a reverse decoy database, employing a stringent FDR cutoff of less than 1%. Proteins identified with a minimum of two unique peptides were considered validly identified proteins. Potential substrate proteins that could interact with OTUD1 were identified.

Western blot and co-immunoprecipitation (co-IP) analysis

A protein extraction kit (Kang Cheng Bioengineering, Shanghai, China), combining cocktails of protease and phosphatase inhibitors (Biosharp, Hefei, China), was used to extract total cell and tissue proteins. The amounts of total protein were measured with a BCA protein test kit (Beyotime, Shanghai, China). The total protein was separated using the SDS-polyacrylamide gel and transferred onto polyvinylidene fluoride membranes (Millipore, Billerica, USA). After blocking with 5% non-fat dried milk, the membrane was incubated with specific primary antibodies, followed by corresponding antibodies conjugated with horseradish peroxidase. Protein bands were visualized using a chemiluminescence kit (G2014, Servicebio) and quantified with ImageJ software. The primary antibodies utilized were: OTUD1, p^{T172}-AMPK (50081, Cell Signaling Technology, MA, USA), p-ACC (3661S, Cell Signaling Technology), ACC (3662S, Cell Signaling Technology), HK-1 (19662-1-AP, Proteintech), AMPK (2532S, Cell Signaling Technology), Grim19 (sc-365978, Santa, USA), SDHA (ab14715, Abcam), UQCRC2 (ab14745, Abcam), MTCO1 (ab14705, Abcam), ATP5A (ab14748, Abcam), CAMkk2 (11549-1-AP, Proteintech), LKB1(10746-1-AP, Proteintech), and GAPDH (60004-1-Ig, Proteintech). The presentation of full scan blots is shown in the Source Data file.

For co-IP experiments, Hek-293T cells underwent co-transfection with designated plasmids. The proteins were isolated from cardiac tissues, primary cardiac muscle cells, or Hek-293T cells using lysis solution for western blot and immunoprecipitation (P0013, Beyotime), along with a mixture of protease inhibitors. The lysis solution was left on ice for 10 min, followed by a spin in a centrifuge to collect the supernatant. Utilizing the BCA assay, the protein concentrations in the cells or heart tissues were quantified. Subsequently, 800 μg of the protein extracts were combined with the respective primary antibody on a shaker at a temperature of 4 °C for an overnight incubation. Protein A/G agarose beads were then introduced into the complexes and subjected to gentle agitation at 4 °C for a duration of 6 h. A fraction of the extracts, one-tenth to be precise, was maintained as Input. After a spin at 1000 × *g* for 5 min, the supernatant was discarded. The beads underwent five times of washing with PBS. The sample was then heated in 2 × SDS loading buffer at 100 °C for 5 min before proceeding to subsequent western blot analysis. Plasmids used included: Flag-OTUD1-WT, Flag-OTUD1-C320A, Flag-OTUD1-delete OTU, Flag-OTUD1-delete UIM, HA-AMPKα2-WT, HA-AMPKα2-delete KD, HA-AMPKα2-delete AID, HA-AMPKα2-delete CTD, HA-AMPKα2-K60R, HA-AMPKα2-K379R, HA-AMPKα2-K391R, HA-AMPKα2-K470R, HA-AMPKα2-K60/379/391R, HA-AMPKα2-K60/379/470R, HA-AMPKα2-K60/391/470R, HA-AMPKα2-K379/391/470R, HA-AMPKα2-K60/379/391/470R, MYC-Ub-WT, MYC-Ub-K48, and MYC-Ub-K63. The primary antibodies used included: Flag-tag antibody, HA-tag antibody (51064-2-AP, Proteintech), MYC-tag antibody (16286-1-AP, Proteintech), mTOR (F0169, Selleck, TX, USA), NRF1 (F11099, Selleck), and VDAC1 (F2882, Selleck).

Deubiquitination assay

In the deubiquitination experiment, Hek293T cells were treated with 10 μM MG132 (T2154, TargetMol, Boston, USA), a protease inhibitor that enhances ubiquitination, for 6 h before harvesting cells. Plasmids containing the specified genes were initially transfected into the Hek-293T cells. Subsequently, the cell lysis was performed using a lysis solution for western blot and immunoprecipitation. Immunoprecipitation was carried out with an HA-tag antibody, followed by the evaluation of ubiquitination levels using immunoblotting.

https://doi.org/10.1038/s41467-025-61901-z

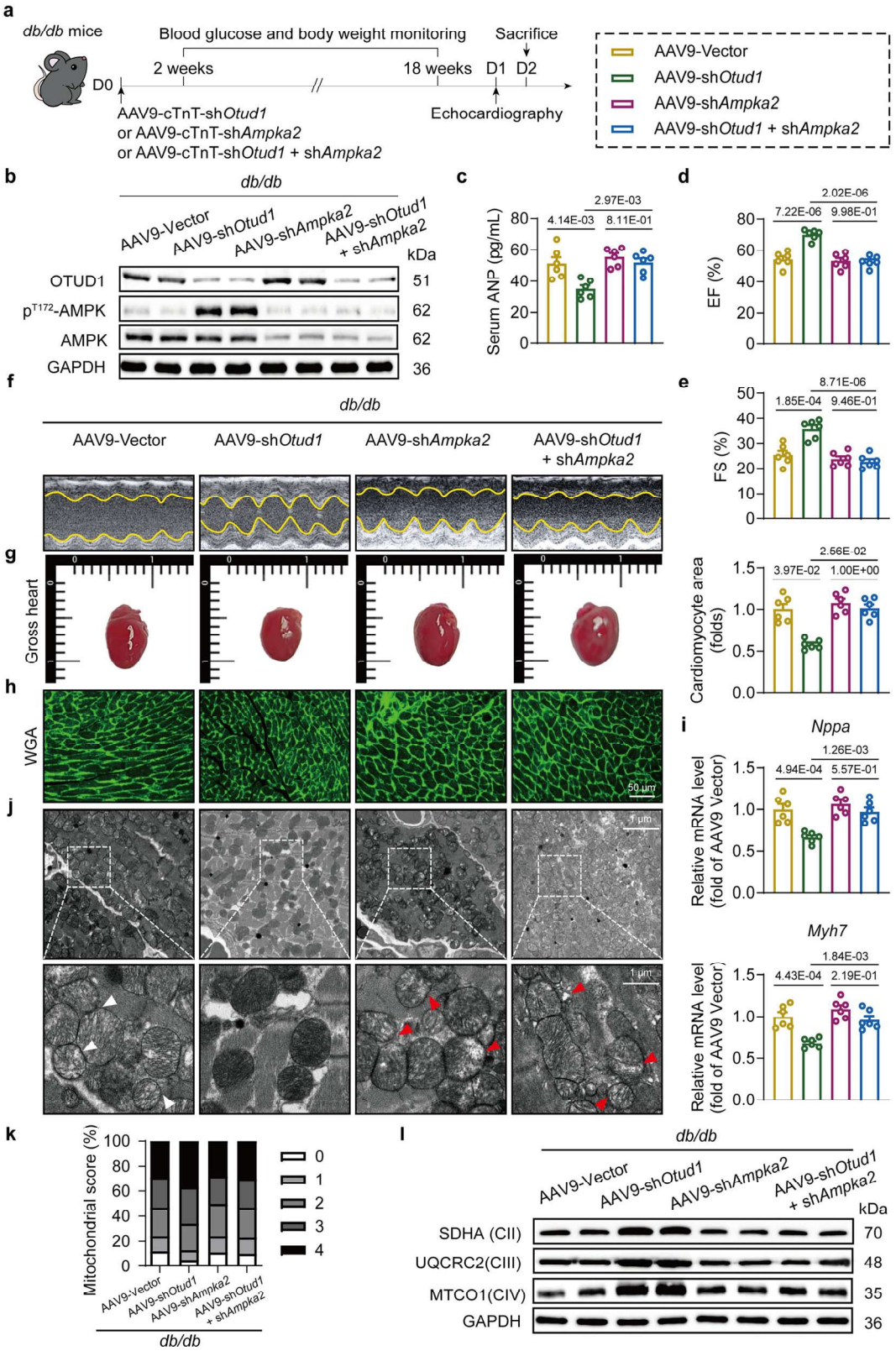

Bio-layer interferometry (BLI)

The BLI analysis was performed using the Octet RED96 System (ForteBio). The running buffer was composed of 150 mM NaCl, 20 mM HEPES (pH 7.5), and 0.02% Tween-20. OTUD1 complexes without ligands, sourced from E. coli BL21 (DE3) ΔhldE, were biotinylated with the EZ-Link Sulfo-NHS-LC-Biotinylation Kit (Thermo Fisher Scientific) for 30 min. These biotinylated complexes were immobilized on a Super Streptavidin (SSA) biosensor that had been pre-equilibrated in the running buffer for 10 min. Subsequently, the SSA biosensor was introduced into a buffer containing AMPKα2 (Abiocenter Biotechnology, Wuxi, China) at the specified concentration for association, or into a buffer without the analyte for dissociation. The data was analyzed, and the binding constant was determined using software supplied by Fortebio.

Fig. 8 | Cardiac AMPKα2 knockdown abolishes the cardioprotective effects of OTUD1 deficiency in diabetic mice. a Adeno-associated virus 9 (AAV9) carrying shRNAs targeting *Otud1* (AAV9-sh*Otud1*) or *Ampka2* (AAV9-sh*Ampka2*) with the cardiomyocyte-specific promoter cTNT was administered to *db/db* mice via tail vein injection. **b** Western blot analysis of OTUD1 and p^{T172}-AMPK in heart tissues. **c** The levels of serum atrial natriuretic peptide (ANP) in different groups. **d**, **e** Echocardiographic analysis of ejection fraction (EF%) and fractional shortening (FS%) in different groups. **f**, **g** Representative images of echocardiographic and gross heart morphology in each group. **h** Wheat germ agglutinin (WGA) staining and quantitative analysis in heart sections. **i** RT-qPCR analysis of hypertrophic genes in heart tissues. **j** Images of transmission electron microscopy showed mitochondrial morphology in heart tissues from different groups. Red arrows show abnormal mitochondria. **k** Quantitative analysis of mitochondrial morphology scores. **l** Western blot analysis of mitochondrial respiratory chain complex proteins (SDHA, UQCRC2, MTCO1) in heart tissues. For (**h**), scale bar = 50 μm; for (**j**), scale bar = 1 μm. Source data are provided as a Source Data file. Data are presented as mean ± SEM ($n = 6$ for each group); For (**c**–**e**, **i**), *P* values were determined by one-way ANOVA followed by Tukey post hoc tests; For (**h**), *P* values were determined by Kruskal–Wallis test with Dunn post hoc tests.

Statistical analysis and reproducibility

Data were presented as mean ± standard error of mean (SEM), with biological replicates indicated by the number of individuals (n). For comparing between two groups, unpaired two-tailed Student's t-test was applied for normally distributed data with equal variance, Welch's t-test was applied for normally distributed data with unequal variance, and Mann–Whitney U test was performed to non-normal distributed data; For comparing multiple groups of data, one-way analysis of variance (ANOVA) followed by Tukey's multiple comparisons test was applied for normally distributed data with equal variance, and Kruskal–Wallis test with Dunn post hoc tests was performed to analyze distributed with unequal variance and non-normal distribution data. Statistical significance was set at $P < 0.05$. All statistical analyses were performed using GraphPad Prism 8.0 software (GraphPad, CA, USA).

Reporting summary

Further information on research design is available in the Nature Portfolio Reporting Summary linked to this article.

Data availability

The raw bulk RNA-sequencing data have been deposited in the Sequence Read Archive (SRA) under BioProject accession number PRJNA1223556. The single-cell RNA-sequencing datasets are available in the Gene Expression Omnibus (GEO) database under accession code GSE290932. The raw data of mass spectrometry is available at the PRIDE database under accession code PXD061479. Source data are provided with this paper.

References

1. Sheng, S. Y., Li, J. M., Hu, X. Y. & Wang, Y. Regulated cell death pathways in cardiomyopathy. *Acta Pharmacol. Sin.* **44**, 1521–1535 (2023).
2. Huo, J. L. et al. Diabetic cardiomyopathy: early diagnostic biomarkers, pathogenetic mechanisms, and therapeutic interventions. *Cell Death Discov.* **9**, 256 (2023).
3. Ramachandra, C. J. et al. Human-induced pluripotent stem cells for modelling metabolic perturbations and impaired bioenergetics underlying cardiomyopathies. *Cardiovasc. Res.* **117**, 694–711 (2021).
4. Jankauskas, S. S. et al. Heart failure in diabetes. *Metabolism* **125**, 154910 (2021).
5. Peng, C., Zhang, Y., Lang, X. & Zhang, Y. Role of mitochondrial metabolic disorder and immune infiltration in diabetic cardiomyopathy: new insights from bioinformatics analysis. *J. Transl. Med.* **21**, 66 (2023).
6. Qi, B. et al. Akap1 deficiency exacerbates diabetic cardiomyopathy in mice by NDUFS1-mediated mitochondrial dysfunction and apoptosis. *Diabetologia* **63**, 1072–1087 (2020).
7. Ljubkovic, M. et al. Disturbed fatty acid oxidation, endoplasmic reticulum stress, and apoptosis in left ventricle of patients with type 2 Diabetes. *Diabetes* **68**, 1924–1933 (2019).
8. Almeida, E. A., Mehndiratta, M., Madhu, S. V., Kar, R. & Puri, D. PINK1 and oxidative stress in lean and obese patients with type 2 diabetes mellitus. *J. Diabetes Complicat.* **37**, 108542 (2023).
9. Madhavi, Y. V. et al. Targeting AMPK in diabetes and diabetic complications: energy homeostasis, autophagy and mitochondrial health. *Curr. Med. Chem.* **26**, 5207–5229 (2019).
10. Zhou, H. et al. Empagliflozin rescues diabetic myocardial microvascular injury via AMPK-mediated inhibition of mitochondrial fission. *Redox Biol.* **15**, 335–346 (2018).
11. Li, Y. et al. Salidroside protects cardiac function in mice with diabetic cardiomyopathy via activation of mitochondrial biogenesis and SIRT3. *Phytother. Res.* **35**, 4579–4591 (2021).
12. Dewanjee, S. et al. Autophagy in the diabetic heart: a potential pharmacotherapeutic target in diabetic cardiomyopathy. *Ageing Res. Rev.* **68**, 101338 (2021).
13. Madonna, R. et al. Empagliflozin inhibits excessive autophagy through the AMPK/GSK3beta signalling pathway in diabetic cardiomyopathy. *Cardiovasc. Res.* **119**, 1175–1189 (2023).
14. Yang, F. et al. Metformin inhibits the NLRP3 inflammasome via AMPK/mTOR-dependent effects in diabetic cardiomyopathy. *Int. J. Biol. Sci.* **15**, 1010–1019 (2019).
15. Sun, T., Liu, Z. & Yang, Q. The role of ubiquitination and deubiquitination in cancer metabolism. *Mol. Cancer* **19**, 146 (2020).
16. Xiao, X. et al. ERK and USP5 govern PD-1 homeostasis via deubiquitination to modulate tumor immunotherapy. *Nat. Commun.* **14**, 2859 (2023).
17. Kong, C. et al. Triad3A-Mediated K48-Linked ubiquitination and degradation of TLR9 impairs mitochondrial bioenergetics and exacerbates diabetic cardiomyopathy. *J. Adv. Res.* **61**, 65–81 (2024).
18. Ye, B. et al. USP25 Ameliorates Pathological Cardiac Hypertrophy by Stabilizing SERCA2a in Cardiomyocytes. *Circ. Res.* **132**, 465–480 (2023).
19. Ye, B. et al. Deubiquitinase USP25 alleviates obesity-induced cardiac remodeling and dysfunction by downregulating TAK1 and reducing TAK1-mediated inflammation. *JACC Basic Transl. Sci.* **9**, 1287–1304 (2024).
20. Wang, B. et al. Disruption of USP9X in macrophages promotes foam cell formation and atherosclerosis. *J. Clin. Investig.***13**, e154217 (2022).
21. Xie, S. Y. et al. USP28 serves as a key suppressor of mitochondrial morphofunctional defects and cardiac dysfunction in the diabetic heart. *Circulation* **14**, 684–706 (2024).
22. Fan, G. et al. The deubiquitinase OTUD1 noncanonically suppresses Akt activation through its N-terminal intrinsically disordered region. *Cell. Rep.* **42**, 111916 (2023).
23. Oikawa, D. et al. OTUD1 deubiquitinase regulates NF-kappaB- and KEAP1-mediated inflammatory responses and reactive oxygen species-associated cell death pathways. *Cell. Death Dis.* **13**, 694 (2022).
24. Zheng, S. et al. OTUD1 ameliorates cerebral ischemic injury through inhibiting inflammation by disrupting K63-linked deubiquitination of RIP2. *J. Neuroinflamm.* **20**, 281 (2023).
25. Yang, H. et al. Fibroblast growth factor-21 prevents diabetic cardiomyopathy via AMPK-mediated antioxidation and lipid-lowering effects in the heart. *Cell Death Dis.* **9**, 227 (2018).

26. Sundaram, S. et al. Location matters: hexokinase 1 in glucose metabolism and inflammation. *Trends Endocrinol. Metab.* **33**, 665–667 (2022).
27. Deng, X. et al. Celastrol ameliorates lipopolysaccharide (LPS)-induced acute lung injury by improving mitochondrial function through AMPK/PGC-1α/Nrf1-dependent mechanism. *Free Radic. Biol. Med.* **227**, 210–220 (2025).
28. Zhang, H. et al. Nimbolide protects against diabetic cardiomyopathy by regulating endoplasmic reticulum stress and mitochondrial function via the Akt/mTOR pathway. *Tissue Cell* **90**, 102478 (2024).
29. Salin Raj, P. et al. Ferulic acid attenuates high glucose-induced MAM alterations via PACS2/IP3R2/FUNDC1/VDAC1 pathway activating proapoptotic proteins and ameliorates cardiomyopathy in diabetic rats. *Int. J. Cardiol.* **372**, 101–109 (2023).
30. Wang, B. et al. AMPKα2 protects against the development of heart failure by enhancing mitophagy via PINK1 phosphorylation. *Circ. Res.* **122**, 712–729 (2018).
31. Hornbeck, P. V. et al. PhosphoSitePlus, 2014: mutations, PTMs and recalibrations. *Nucleic Acids Res.* **43**, D512–D520 (2015).
32. Wang, M. et al. OTUD1 promotes pathological cardiac remodeling and heart failure by targeting STAT3 in cardiomyocytes. *Theranostics* **13**, 2263–2280 (2023).
33. Wu, S. & Zou, M. H. AMPK, mitochondrial function, and cardiovascular disease. *Int. J. Mol. Sci.* **21**, 4987 (2020).
34. Tiainen, M., Ylikorkala, A. & Mäkelä, T. P. Growth suppression by Lkb1 is mediated by a G (1) cell cycle arrest. *Proc. Natl. Acad. Sci. USA* **96**, 9248–9251 (1999).
35. Bai, T., Wang, F., Mellen, N., Zheng, Y. & Cai, L. Diabetic cardiomyopathy: role of the E3 ubiquitin ligase. *Am. J. Physiol. Endocrinol. Metab.* **310**, E473–E483 (2016).
36. Yan, M. et al. USP7 promotes cardiometabolic disorders and mitochondrial homeostasis dysfunction in diabetic mice via stabilizing PGC1β. *Pharmacol. Res.* **205**, 107235 (2024).
37. Wang, Q. et al. OTUD1 promotes isoprenaline- and myocardial infarction-induced heart failure by targeting PDE5A in cardiomyocytes. *Biochim. Biophys. Acta Mol. Basis Dis.* **1870**, 167018 (2024).
38. Lu, H., Xie, Y., Zhou, Z., Hong, P. & Chen, J. Identification of novel targets for treatment of dilated cardiomyopathy based on the ferroptosis and immune heterogeneity. *J. Inflamm. Res.* **16**, 2461–2476 (2023).
39. Yao, F. et al. SKP2- and OTUD1-regulated non-proteolytic ubiquitination of YAP promotes YAP nuclear localization and activity. *Nat. Commun.* **9**, 2269 (2018).
40. Trefts, E. & Shaw, R. J. AMPK: restoring metabolic homeostasis over space and time. *Mol. Cell* **81**, 3677–3690 (2021).
41. Stapleton, D. et al. Mammalian AMP-activated protein kinase subfamily. *J. Biol. Chem.* **271**, 611–614 (1996).
42. Wang, D. et al. $FGF1^{\Delta HBS}$ prevents diabetic cardiomyopathy by maintaining mitochondrial homeostasis and reducing oxidative stress via AMPK/Nur77 suppression. *Signal Transduct. Target. Ther.* **6**, 133 (2021).
43. Lu, Q. B. et al. Metrnl ameliorates diabetic cardiomyopathy via inactivation of cGAS/STING signaling dependent on LKB1/AMPK/ULK1-mediated autophagy. *J. Adv. Res.* **51**, 161–179 (2023).
44. Jiang, P. et al. Negative regulation of AMPK signaling by high glucose via E3 ubiquitin ligase MG53. *Mol. Cell* **81**, 629–637 (2021).
45. He, H. et al. Metformin and systemic metabolism. *Trends Pharmacol. Sci.* **41**, 868–881 (2020).
46. Akter, H. et al. Metformin ameliorates neuroinflammatory environment for neurons and astrocytes during in vitro and in vivo stroke and tobacco smoke chemical exposure: role of Nrf2 activation. *Redox Biol.* **75**, 103266 (2024).
47. Steinberg, G. R. & Hardie, D. G. New insights into activation and function of the AMPK. *Nat. Rev. Mol. Cell Biol.* **24**, 255–272 (2023).
48. Qi, J. et al. Downregulation of AMP-activated protein kinase by Cidea-mediated ubiquitination and degradation in brown adipose tissue. *EMBO J.* **27**, 1537–1548 (2008).
49. Ko, J. R. et al. Aerobic exercise training decreases cereblon and increases AMPK signaling in the skeletal muscle of STZ-induced diabetic rats. *Biochem. Biophys. Res. Commun.* **501**, 448–453 (2018).
50. Sha, B. et al. USP8 inhibitor-induced DNA damage activates cell cycle arrest, apoptosis, and autophagy in esophageal squamous cell carcinoma. *Cell Biol. Toxicol.* **39**, 2011–2032 (2023).
51. Li, J. et al. LncRNAs are involved in regulating ageing and age-related disease through the adenosine monophosphate-activated protein kinase signalling pathway. *Genes Dis.* **11**, 101042 (2023).
52. Medzikovic, L. et al. Connecting sex differences, estrogen sig-naling, and microRNAs in cardiac fibrosis. *J. Mol. Med.* **97**, 13851–398 (2019).

Acknowledgements

This study was supported by the National Natural Science Foundation of China (81930108 to G. Liang), the Natural Science Foundation of Zhejiang Province (LTGD24C040007 to Q.S.), and the Medical Scientific Research Foundation of Zhejiang Province (Grants No. 2024KY932 to X.H.). We appreciate the PTM BIO company for offering us the $AMPK\alpha2^{-/-}$ H9C2 cells.

Author contributions

X.H. and G. Liang drafted and revised the manuscript; X.H., R.Z., J. Zhang, Y.L., Z. Li, G. Liu, W.L., Z. Liang, M.W., and G. Liang designed and performed the experiments. R.Z., J. Zheng, and J.Y. generated cardiomyocyte-specific *Otud1* knockout mice. Q.S., H.Y., and G. Liang supervised the work. All authors approved the final version of the manuscript.

Competing interests

The authors declare no competing interests.

Additional information

Supplementary information The online version contains supplementary material available at https://doi.org/10.1038/s41467-025-61901-z.

Correspondence and requests for materials should be addressed to Qiaojuan Shi, Huazhong Ying or Guang Liang.

Peer review information *Nature Communications* thanks Brian Rodrigues and the other, anonymous, reviewer for their contribution to the peer review of this work. A peer review file is available.